AFRL-DE-PS-
TR-2004-1138

THE MEASUREMENT OF GAIN IN A SUPERSONIC, COMBUSTION-DRIVEN GENERATOR FOR NCl($a^1\Delta$)

Gerald C. Manke II, et. al.

4 February 2005

Final Report

AIR FORCE RESEARCH LABORATORY
Directed Energy Directorate
3550 Aberdeen Ave SE
AIR FORCE MATERIEL COMMAND
KIRTLAND AIR FORCE BASE, NM 87117-5776

STINFO COPY

Using Government drawings, specifications, or other data included in this document for any purpose other than Government procurement does not in any way obligate the U.S. Government. The fact that the Government formulated or supplied the drawings, specifications, or other data, does not license the holder or any other person or corporation; or convey any rights or permission to manufacture, use, or sell any patented invention that may relate to them.

This report has been reviewed by the Public Affairs Office and is releasable to the National Technical Information Service (NTIS). At NTIS, it will be available to the general public, including foreign nationals.

If you change your address, wish to be removed from this mailing list, or your organization no longer employs the addressee, please notify AFRL/DELC, 3550 Aberdeen Ave SE, Kirtland AFB, NM 87117-5776.

Do not return copies of this report unless contractual obligations or notice on a specific document requires its return.

This report has been approved for publication.

//signed//

GERALD C. MANKE II, DR-II
Principle Investigator

//signed//

KIP R. KENDRICK, DR-III
Chief, High Power Gas Lasers Branch

//signed//

L. BRUCE SIMPSON, SES
Director, Directed Energy

REPORT DOCUMENTATION PAGE

Form Approved
OMB No. 0704-0188

1. REPORT DATE *(DD-MM-YYYY)*	**2. REPORT TYPE**	**3. DATES COVERED** *(From - To)*
04-02-2005	Final Report	1 Oct 2003 – 30 Dec 2004

4. TITLE AND SUBTITLE

The Measurement of Gain in a Supersonic, Combustion-Driven Generator for $NCl(a^1\Delta)$

5a. CONTRACT NUMBER
N/A

5b. GRANT NUMBER
N/A

5c. PROGRAM ELEMENT NUMBER
N/A

6. AUTHOR(S)
Gerald C. Manke II, Timothy J. Madden, Chris B. Cooper, Shiv C. Dass, and Gordon D. Hager

5d. PROJECT NUMBER
4866

5e. TASK NUMBER
LB

5f. WORK UNIT NUMBER
10

7. PERFORMING ORGANIZATION NAME(S) AND ADDRESS(ES)

Air Force Research Laboratory
3550 Aberdeen Avenue SE
Kirtland AFB, NM 87117-5776

8. PERFORMING ORGANIZATION REPORT NUMBER

9. SPONSORING / MONITORING AGENCY NAME(S) AND ADDRESS(ES)

10. SPONSOR/MONITOR'S ACRONYM(S)

11. SPONSOR/MONITOR'S REPORT NUMBER(S)
AFRL-DE-PS-TR-2004-1138

12. DISTRIBUTION / AVAILABILITY STATEMENT

Approved for public release; distribution is unlimited

13. SUPPLEMENTARY NOTES

14. ABSTRACT

The measurement of positive small signal gain on the 1.315 micron spin orbit transition of atomic iodine following energy transfer from chemically generated $NCl(a^1\Delta)$ is reported. Previous instances of gain produced by energy transfer from $NCl(a^1\Delta)$ used DC discharges to generate F and Cl atoms; this report describes recent progress towards a true chemical laser device which uses a high temperature chemical combustor and a supersonic reactor to generate $NCl(a^1\Delta)$. These improvements represent a significant step towards the development and demonstration of a scalable All Gas-phase Iodine Laser (AGIL) device.

15. SUBJECT TERMS
Chemical lasers, AGIL, All Gas-phase iodine laser, COIL

16. SECURITY CLASSIFICATION OF:			**17. LIMITATION OF ABSTRACT**	**18. NUMBER OF PAGES**	**19a. NAME OF RESPONSIBLE PERSON**
a. REPORT	**b. ABSTRACT**	**c. THIS PAGE**			Gerald C. Manke II
Unclassified	Unclassified	Unclassified	SAR	52	**19b. TELEPHONE NUMBER** *(include area code)* (505) 853-2674

Standard Form 298 (Rev. 8-98)
Prescribed by ANSI Std. 239.18

Table of Contents

List of Figures

List of Tables

Acknowledgements

The authors wish to acknowledge extensive helpful discussions with Prof. Michael Heaven (Emory University), Dr. Steven J. Davis (Physical Sciences, Inc), and Mr. Peter G. Crowell (Northrop Grumman, IT). The NCl($X^3\Sigma^-$) diagnostic was provided as a result of USAF SBIR funding via contract #F29601-00-C-0053. Finally, the supersonic AGIL program has benefited in countless ways from the hard work, dedication, and skills of Dr. Shiv Dass, Ms. Norma McMackin, Mr. Richard Dow, and Mr. Richard Hagenloh.

Introduction

The All Gas-phase Iodine Laser (AGIL)[1-4] is a laser device and concept which uses near resonant energy transfer from an electronically excited molecule, $NCl(a^1\Delta)$, to ground state atomic iodine to produce an inversion on the 1.3154 μm spin orbit transition of iodine.

$$NCl(a^1\Delta) + I(^2P_{3/2}) \rightarrow NCl(X^3\Sigma^-) + I^*(^2P_{1/2}) \quad (1)$$

This concept is an all-gas phase variant of the chemical oxygen iodine laser (COIL) which uses the energy transfer between electronically excited oxygen, $O_2(a^1\Delta)$, and atomic iodine to produce $I^*(^2P_{1/2})$[5]:

$$O_2(a^1\Delta) + I(^2P_{3/2}) \rightarrow O_2(X^3\Sigma^-) + I^*(^2P_{1/2}). \quad (2)$$

It is possible to substitute $NCl(a^1\Delta)$ for $O_2(a^1\Delta)$ because both molecules possess an $(p\pi^*)^2 (p\sigma^*)^0$ electronic configuration (and therefore, have the same electronic states), are metastable, and have large branching fractions for the near-resonant energy transfer to atomic iodine. While COIL is a relatively efficient laser (in terms of W/kg and compared to other high energy laser technologies), it suffers from complicated engineering challenges related to the use of two-phase chemistry in the production of $O_2(a^1\Delta)$. The reaction of molecular chlorine with an aqueous solution of basic hydrogen peroxide (BHP) produces $O_2(a^1\Delta)$ with near-unit efficiency,

$$Cl_2 + H_2O_2 + 2OH^- \rightarrow O_2(a^1\Delta) + 2H_2O + 2Cl^- \quad (3)$$

The use of a two-phase reactor and some unfavorable secondary chemistry (e.g. H_2O efficiently quenches $I^*(^2P_{1/2})$) leads to complex and severe engineering challenges for large-scale, high-energy devices, particularly those that require mobility. AGIL is an attractive potential alternative to COIL because $NCl(a^1\Delta)$ can be generated by reactions that occur solely in the gas phase.

The history and development of COIL has been well documented by McDermott[6], Heaven[7], and others[8]. The first continuous wave AGIL device, demonstrated by Henshaw in 2000[3], was enabled and inspired by the work of many, including Benard[9], Bower[10, 11], Clyne[12-14], Coombe and Gilbert[15-19], Heaven[7, 20, 21], Henshaw[22, 23], Herbelin[4], Manke[24, 25], and Setser[26-31]. Most recently, multi-watt laser demonstrations were performed by the AGIL team at the Air Force Research Laboratory [1, 2] using a 20 cm wide subsonic reactor that used a series of 4 DC discharges to produce the requisite F and Cl atoms. The highest gain and power measured on the 20 cm device were 4.2×10^{-4} cm^{-1} and 31 W, respectively[32]. In addition to the AFRL work, the Short Wavelength Chemical Laser Laboratory in Dalian, China continues to pursue AGIL technology[33].

Successful AGIL gain and laser demonstrations have produced $NCl(a^1\Delta)$ via a two step reaction of chlorine atoms with hydrogen azide[24, 27, 28, 31]:

$$Cl + HN_3 \rightarrow HCl + N_3 \quad (4)$$

$$Cl + N_3 \rightarrow NCl(a^1\Delta) + N_2 \quad (5)$$

The chlorine atoms were generated by the reaction of atomic fluorine and DCl,

$$F + DCl \rightarrow DF + Cl, \quad (6)$$

where the F atoms were generated by a DC discharge of molecular fluorine and/or NF_3 diluted in He. To improve the chemical efficiency of AGIL, small flows of hydrogen iodide are reacted with atomic fluorine or chlorine to produce $I(^2P_{3/2})$ prior to the reaction with hydrogen azide so that the $I(^2P_{3/2})$ atoms will be present as soon as $NCl(a^1\Delta)$ is produced.

$$F + HI \rightarrow HF + I(^2P_{3/2}) \quad (7)$$

$$Cl + HI \rightarrow HCl + I(^2P_{3/2}) \quad (8)$$

Unfortunately, the F atom production efficiency of the DC discharges declines as a function of the flow rate of the F-atom source[34]; the technology that was used to previously demonstrate the AGIL concept is not suitable for the development or demonstration of a kW-scale device. This paper describes our efforts to generate $NCl(a^1\Delta)$, $I^*(^2P_{1/2})$, and observe small signal gain using chemical combustor technology for the generation of $NCl(a^1\Delta)$.

The experimental regimes examined by this work and previous AFRL AGIL programs are summarized in Table 1.

Table 1. Comparison of AGIL Devices.

	AGIL 1 (Herbelin)[4]	**AGIL 1A (Henshaw)[3]**	**AGIL 2 (Manke)[1, 32]**	**Supersonic AGIL (this work)**
Reactor Properties				
F atom source	1 DC discharge	1 DC discharge	4 DC discharges	$D_2/F_2/NF_3$ combustor
Flow speed	M < 1	M < 1	M ~ 1	M = 3.5
Path length (cm)	5	5	20	5
Pressure (Torr)	16	15 - 16	20 - 30	200 – 350[b] 3 – 12[c]
Power (W)	NA	180 mW	31 W	NA
Gain (cm^{-1})	2.0×10^{-4}	2.6×10^{-4}	4.2×10^{-4}	1.4×10^{-4}
Flow Rates (mmol s^{-1})				
He	150	150	480 – 1000	50 – 250[a]
F_2	0.66	NA	2 - 8	10
NF_3	NA	1 – 1.5	4 - 20	0 – 20
D_2	NA	NA	NA	2.5 – 20
DCl	2.0	2.0 – 2.5	15 - 25	30 – 70
HI	0.03	0.04 – 0.07	0.12 – 0.60	0.2 – 1.0
HN_3	3.32	3.0 – 4.5	10 - 70	10 – 70

[a] He added to combustor only, total He is sum of this value and 9 times the HN_3 flow rate
[b] static combustor pressure
[c] static pressure in supersonic flow channel

Experimental Methods

Experimental Apparatus

The supersonic AGIL device consisted of three major components, a subsonic $D_2/F_2/NF_3$/DCl/HI combustor, a converging – diverging nozzle and HN_3 injector, and a supersonic flow chamber, see Figures 1 - 2.

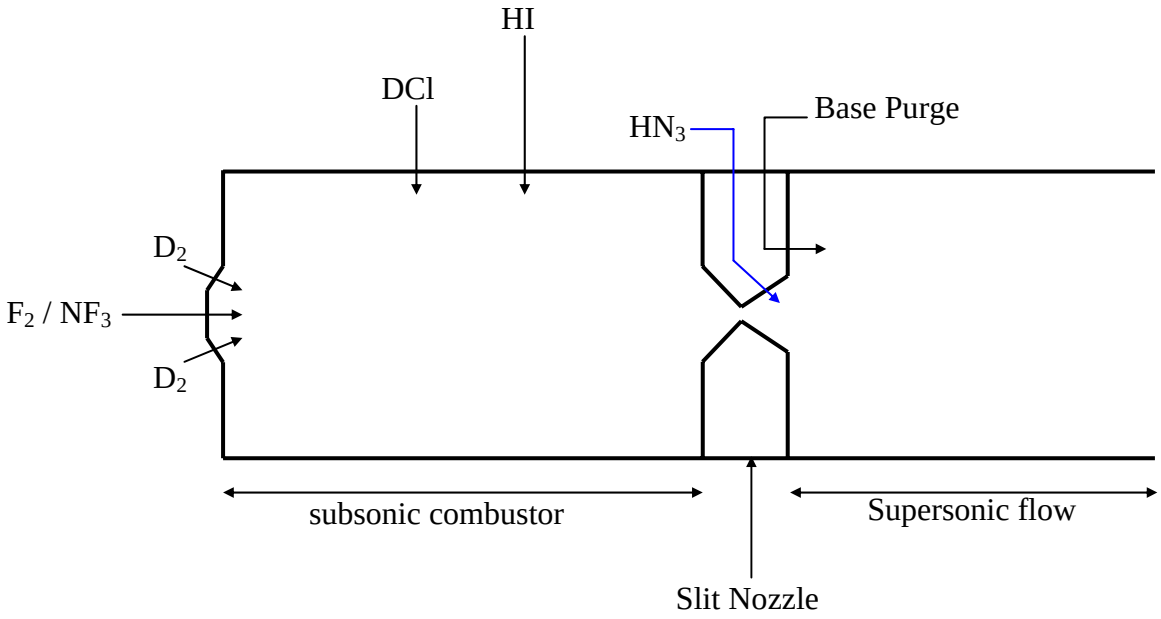

Figure 1. Supersonic AGIL hardware.

The combustion chamber measured 3.3 cm high, 5 cm wide, and 5.5 cm deep. Injectors for D_2 and F_2/NF_3 were located on the back wall of the combustion chamber. The D_2 injector consisted of two rows of 6 holes, each 0.038 cm in diameter. Molecular fluorine and nitrogen trifluoride were mixed upstream of the combustor and injected through a single row of 6 holes, each 0.132 cm in diameter. The D_2 injectors were located 0.38 cm above and below the row of F_2/NF_3 injector holes. The total injector areas for D_2 and F_2/NF_3 were 0.014 and 0.082 cm^2, respectively. The DCl and HI injectors were located on the top and bottom walls of the combustion chamber. The DCl injector block was placed 2.0 cm from the back wall and consisted of two rows of 36 holes (i.e. one row each for the top and bottom), each 0.056 cm in

diameter. The total DCl injector area was 0.177 cm^2. The HI injector was placed 3.5 cm from the back wall and consisted of two rows of 54 holes (i.e. one row each for the top and bottom), each 0.033 cm in diameter. The total HI injector area was 0.0925 cm^2.

Four different supersonic nozzles were employed in this work. In all cases, the nozzle consisted of a 5 cm wide slit, with the throat placed 7.0 cm from the back wall of the combustion chamber. Table 2 summarizes the geometry of the nozzles used in this study.

Table 2. Supersonic AGIL nozzles specifications

Nozzle	Throat height (cm)	Nozzle Angle	A/A* (Mach #)[a]	HN_3 injector area (cm^2) HN_3 injector hole diameter (cm)
A	0.46	40	3.45 (3.2)	0.195 0.101
B	0.46	40	3.45 (3.2)	0.630 0.183
C	0.23	20	3.35 (3.2)	0.630 0.183
D[b]	0.46	40	3.45 (3.2)	0.630 0.183

[a] Calculated by iteratively solving equation (11) for M using the measured A/A* ratio and assuming $\gamma = 1.667$.
[b] Nozzle D injected HN_3 into the subsonic portion of the flow, 0.74 cm upstream of the throat.

Nozzles A,B, and D had a 0.46 cm throat height and 40 degree expansion angle. The throat for nozzle C was a factor of 2 smaller but maintained approximately the same A/A* ratio (and Mach number) by having a smaller expansion angle, 20 degrees. In all cases, the nozzle expansion extended for 1.55 cm past the nozzle throat. For nozzles A – C hydrogen azide was injected 0.4 cm downstream of the nozzle throat (i.e. 7.4 cm from the back wall of the combustion chamber) through 2 rows of 12 holes (1 row each, top and bottom). Nozzle D, on the other hand, incorporated HN_3 addition 0.74 cm upstream of the throat, into the subsonic combustion

chamber. The HN_3 injector holes for Nozzle A were 0.102 cm in diameter while the individual injector holes for Nozzles B – D were 0.183 cm in diameter.

The supersonic flow chamber begins at the nozzle exit plane and extends downstream to the end of the reactor. The vertical height of the flow chamber was 3.3 cm. Because this height exceeds the height of the nozzle at the nozzle exit plane, a He injector was installed into the face of the nozzle to discourage recirculation of the reactive flow in the base purge region, see Figure 1. In addition to the base purge, a pair of supersonic ($M \geq 5$) bank blower injectors were placed on either side of the nozzle to prevent expansion of the flow beyond the 5 cm width defined by the slit. Pitot probe measurements across the face of the nozzle confirmed flow containment and a 5 cm path length for the supersonic portion of the flow, see below.

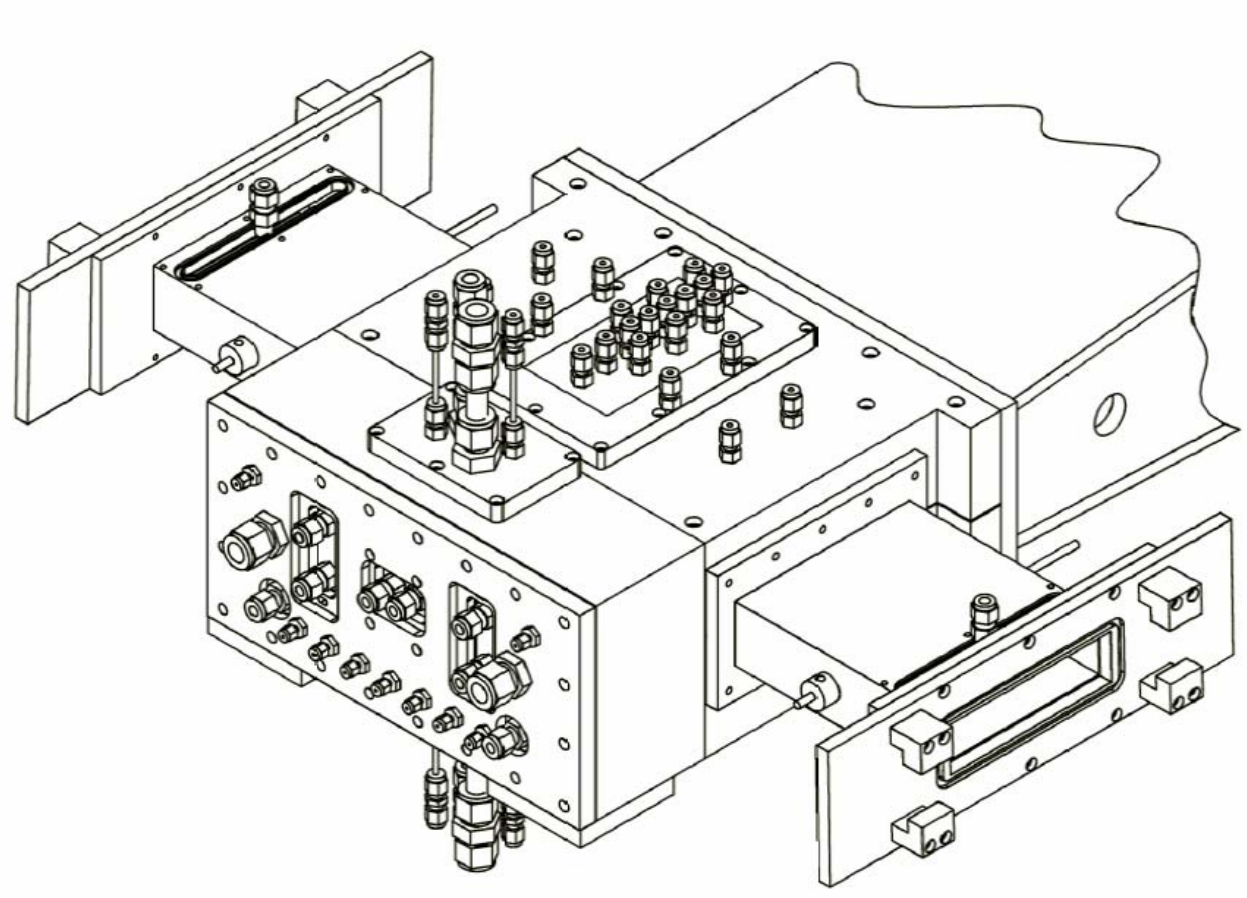

Figure 2. Assembly drawing of supersonic AGIL reactor.

Mirror tunnels were constructed and attached to the sides of the reactor to allow flow visualization as well as small signal gain measurements. For most of the experiments described in this report, the mirror tunnels allowed observation of a 12 cm long region of the flow. Based on the observation that the highest gain was found at the end of the 12 cm observation zone, a second pair of mirror tunnels were installed. The second set of tunnels provided a 25 cm long observation zone. In both cases, a purge flow of He was added to each tunnel to help prevent damage by the corrosive gas to the glass windows.

All reagent and diluent flow rates except for HN_3 were controlled by Proportion Air electronic gas pressure regulators (Model #QBIT-FEE-500) and calibrated sonic orifices. Pressures were monitored with MKS Baratron (Model 622-A) and Druck (PMP 1265) pressure transducers while temperatures were measured with Omega (Type T) thermocouples. A National Instruments Labview program was used to control and record all reactor conditions for later analysis. The HN_3 flow was "controlled" by filling a pair of 150 L stainless steel tanks to a specified pressure with a 10% HN_3 in He mixture and applying the full pressure of the tanks to the plenum of the HN_3 injectors. The average flow rate of HN_3 for each experiment was calculated from the measured pressure drop in the reservoir tanks. Typical flow rates are shown in Table 1. Typical conditions from previous AGIL devices are also given in Table 1 for comparison.

Diagnostics

Visible and near-infrared (NIR) emission spectra were observed with a 0.3 m monochromator (Acton, SpectroPro 300i) and a combination of 2 optical multi-channel analyzers. The NIR emissions were collected with a liquid nitrogen cooled 512-pixel InGaAs array (Roper Scientific, OMA V) while the visible emissions were collected with a liquid

nitrogen cooled 1340 x 100 pixel CCD (Roper Scientific, Spec 10:100BR). Binning the 100 pixels along the vertical axis created a single row of 1340 "superpixels". In addition to the spectroscopic measurements, a video camera provided visual images of the flow stream.

The F / Cl atom production efficiency was determined by a series of gas phase titrations with HCl[1]. Briefly, a tunable external cavity diode laser (New Focus, Model 6248) was tuned to the P(3) ro-vibrational line of the HF (0-2) overtone spectrum; the absorption was measured as a function of HCl added to the high temperature combustor. The absorption increases linearly with HCl until all of the F atoms are consumed. The titration endpoint is reached when additions of HCl no longer lead to increased absorption and the initial F atom flow rate is equal to the corresponding HCl flow rate. The small signal gain on the $I(^2P_{3/2}) - I^*(^2P_{1/2})$ transition was monitored by the same diode laser tuned to the F(3,4) hyperfine transition. The initial I atom density was measured prior to HN_3 addition to determine $[I_{tot}]$.

Finally, a tunable 664 nm diode laser was used to probe the density of $NCl(X^3\Sigma^-)$. This diagnostic device was developed and delivered to the AFRL via a Phase II SBIR contract with Physical Sciences, Inc[35]. The laser was continuously scanned from 15049 to 15050 cm^{-1} (664.46 – 664.48 nm) through a spectral region that contains 2 hyperfine lines of the $NCl(X^3\Sigma^-) - NCl(b^1\Sigma^+)$ spectrum[21], $^QR(15)$ and $^QP(15)$. The absolute wavelength and frequency axis of the spectrum were calibrated by simultaneously collecting a high-resolution spectrum of molecular I_2. The density of $NCl(X^3\Sigma^-)$ is calculated from the integrated absorption area and the calculated value for the transition-specific line strength[35].

Experimental Results

Pitot Probe measurements

Pitot probe measurements were performed across the face of the nozzle and bank blowers to verify supersonic flow as well as containment within the 5 cm area defined by the nozzle width and bank blowers. The results for Nozzle A/B are shown in Figure 3. The probe was raked across the flow in 5 mm increments. The Mach number was calculated from the measured pitot pressure, static (sidewall) pressure, and equation (9)

$$M = \sqrt{\frac{2}{\gamma - 1}\left[\left(\frac{P_0}{P}\right)^{\frac{\gamma-1}{\gamma}} - 1\right]}, \tag{9}$$

where P_0 is the stagnation (pitot) pressure, P is the static (cavity sidewall) pressure, γ is the specific heat ratio (C_p/C_v), and M is the Mach number.

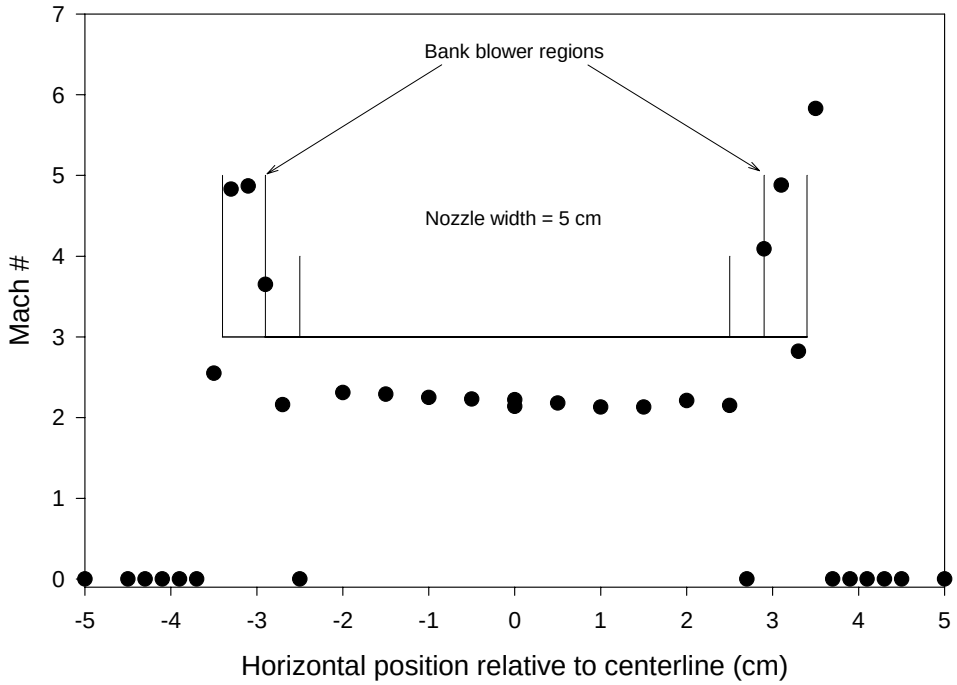

Figure 3. Pitot Probe Results for Nozzle A/B.

The data is consistent with a 5 cm wide supersonic channel with M > 2, bounded on either side by a relatively narrow region where M >4. The M > 4 regions correspond to the bank blowers. Beyond the bank blowers is a pressure matched subsonic flow region. Although the pitot probe measurements for the Mach number do not precisely completely agree with the Mach number predicted by the A/A* ratio (see below), they conclusively demonstrated that the nozzle was choked and that the flow was reasonably well behaved under cold flow conditions.

Vertical Profiles of combustion products

Vertical profiles of the flow generated by Nozzles A – C were performed prior to the addition of HN_3. Results for Nozzle A/B are shown in Figures 4 and 5, while Nozzle C results are shown in Figure 6. Because symmetry about the vertical axis was assumed, the data shown for the region above the vertical centerline are the same as the measured values from below the vertical centerline. The experimental conditions for Figure 4 were F_2 = 12.5, D_2 = 5.0, and HCl = 50 mmol s^{-1}. HF overtone absorptions were measured along the vertical centerline at x = 2 and 7 cm downstream of the Nozzle Exit Plane (NEP). Injecting HCl rather than DCl and using the HF absorption rather than I atom absorption allowed us to determine whether the Cl atom source (i.e. DCl) was fully penetrating into the combustor flow and whether the F and Cl atoms were uniformly distributed across the nozzle face.

Although there is considerable scatter, the data show that the bulk of the flow is contained within ± 8 mm of the vertical centerline, even at the furthest downstream point that was probed. Similar to the [HF(v = 0)] plot in the upper panel, the temperature plot also shows a significant amount of scatter. The general trend, however, is consistent with a well defined supersonic expansion. Interestingly, slightly higher temperatures are observed in the base purge region – most likely due to equilibration with the room temperature base purge He flow.

Figure 5 shows a vertical profile of atomic iodine from the same nozzle. The experimental conditions were D_2 = 10, F_2 = 12, NF_3 = 15, DCl = 40, and HI = 1.2 mmol s^{-1}. This data was generated by adding HI to the combustor's F/Cl atom flow and monitoring the I($^2P_{3/2}$) – I*$^2P_{1/2}$) absorption at 1.315 μm. By monitoring the I atom absorption, we were able to confirm that the HI injectors were fully penetrating into the combustor flow and that the I atoms were also evenly distributed in the output of the supersonic nozzle.

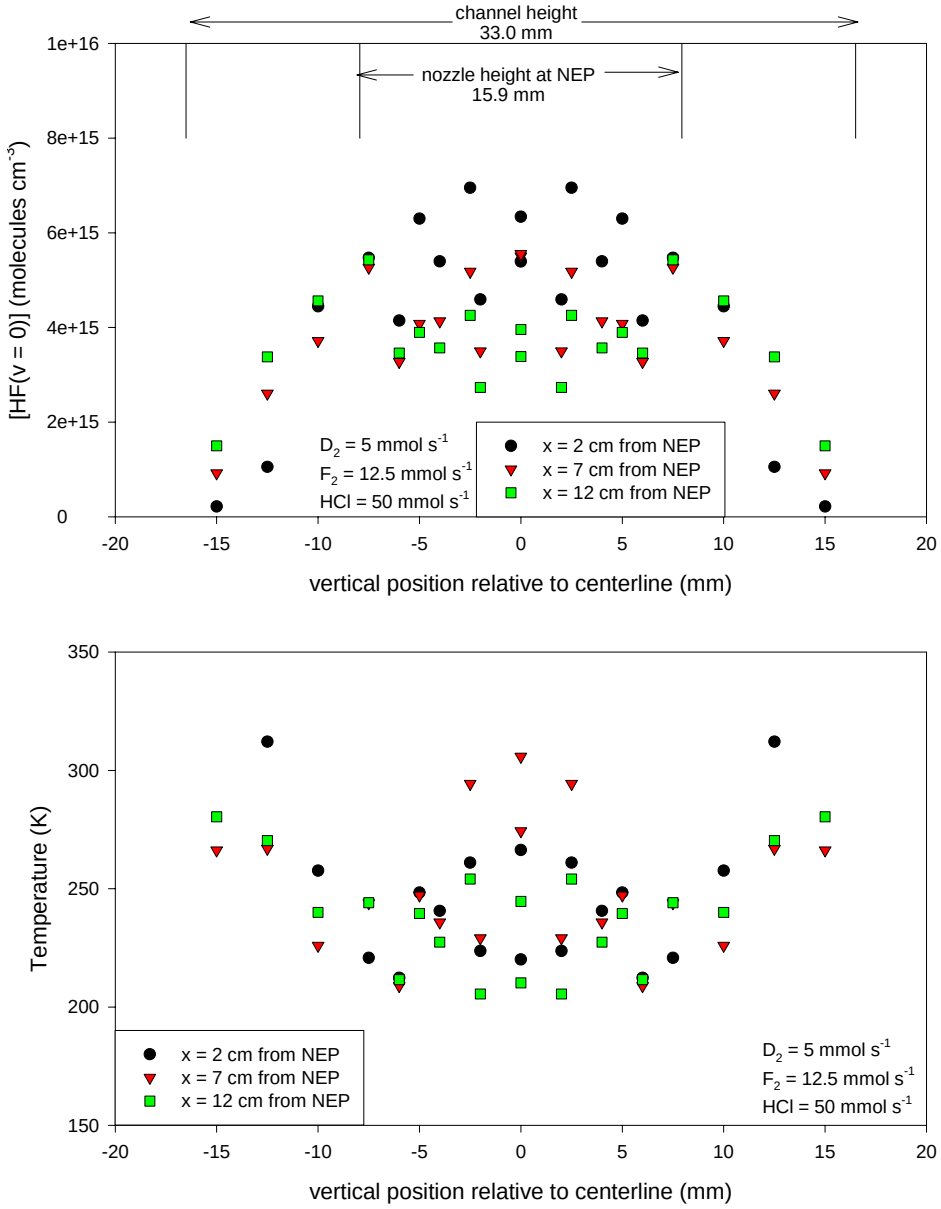

Figure 4. Vertical profiles for Nozzle A/B – HF(2-0) absorption and temperature.

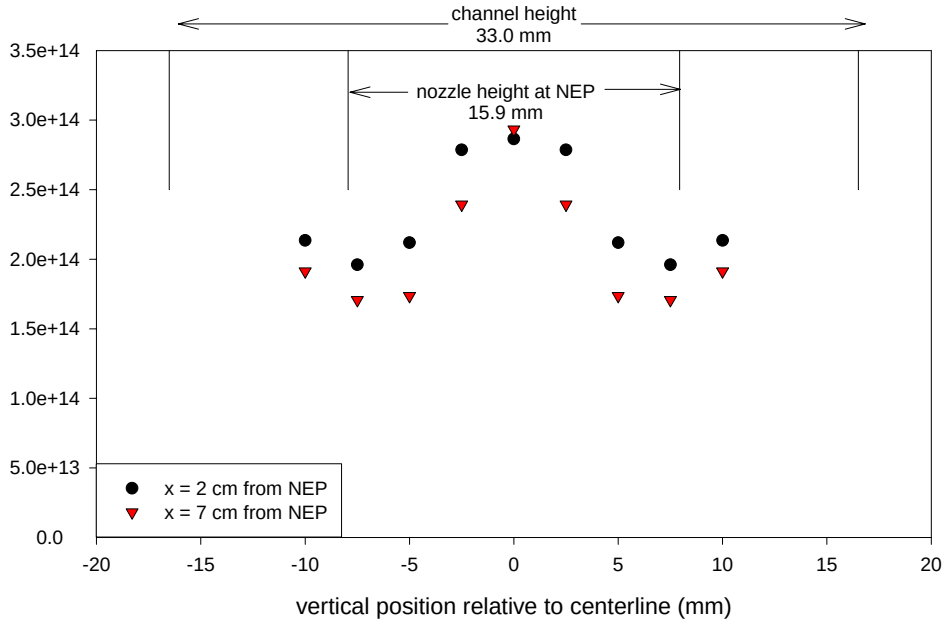

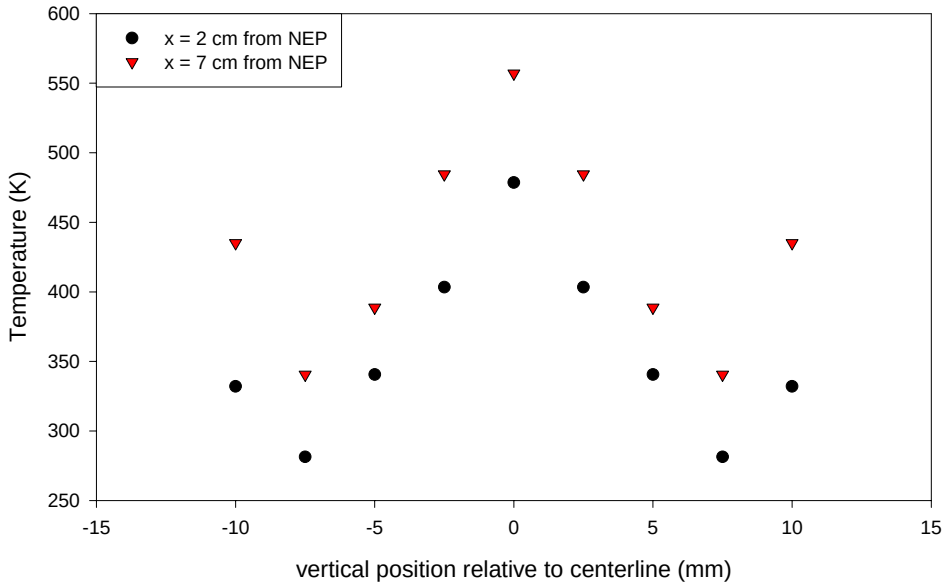

Figure 5. Vertical profiles for Nozzle A/B – I atom absorption and temperature.

Finally, a vertical profile for Nozzle C is shown in Figure 6. The experimental conditions for this test were D_2 = 7.5, F_2 = 10, NF_3 = 10, DCl = 70, and HI = 0.2 mmol s^{-1}. The [I_{tot}] and temperatures are similar to the results from Nozzle A/B and again clearly show that the I atoms have fully penetrated the flow and are distributed across the face of the nozzle.

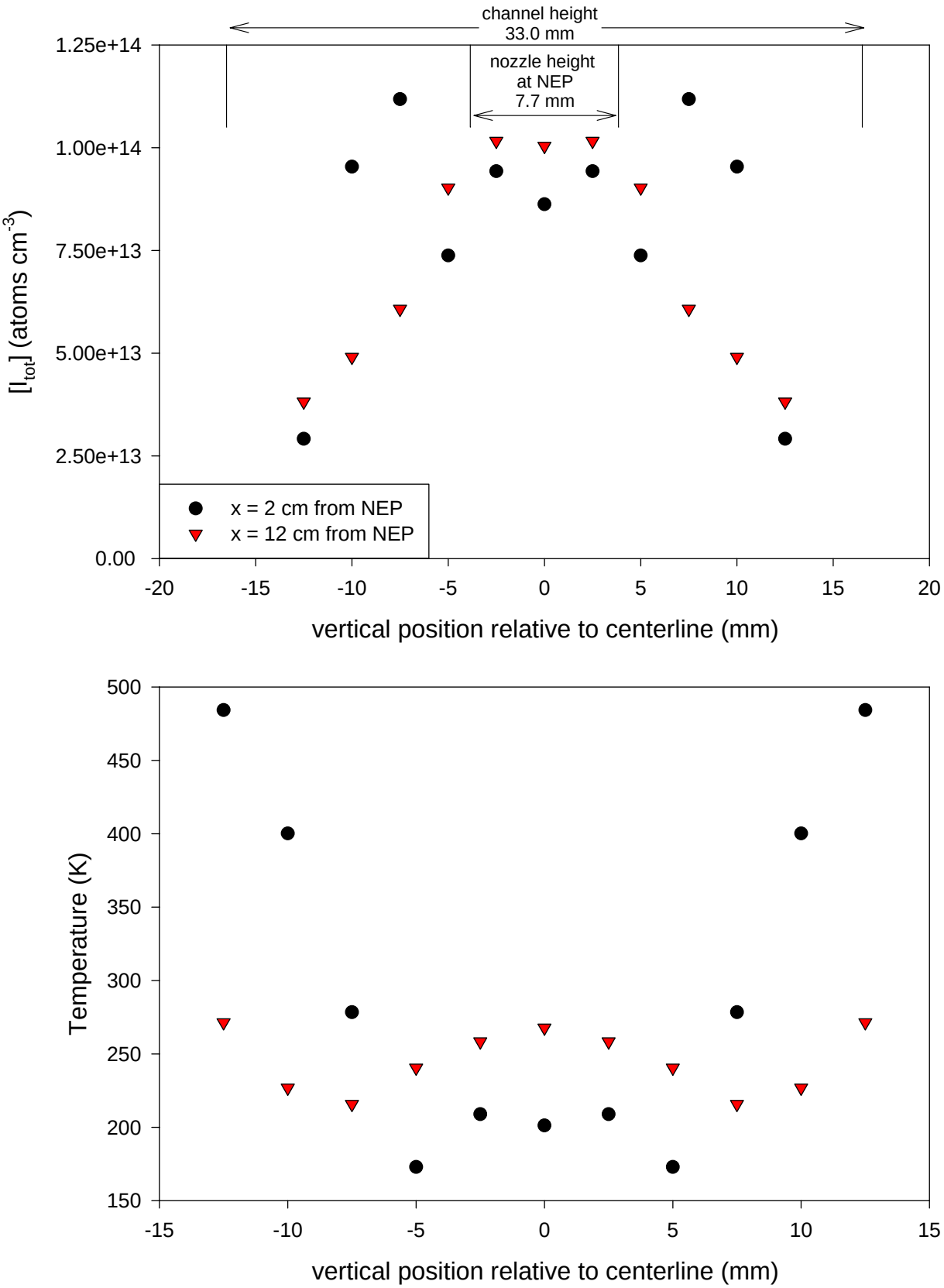

Figure 6. Vertical profiles for Nozzle C – I atom absorption and temperature.

F atom titrations

Gas-phase titrations were performed as described above to determine the initial F atom density produced by the high temperature combustor. A sample titration is shown in Figure 7 for Nozzle A and F_2 = 12, D_2 = 10, NF_3 = 5, and He = 125 mmol s^{-1}. A slight break to the linear growth of the absorption signal indicates the titration endpoint at approximately 17 mmol s^{-1}. Surprisingly, the titration results are not nearly as clear as those generated by the subsonic AGIL experiments.

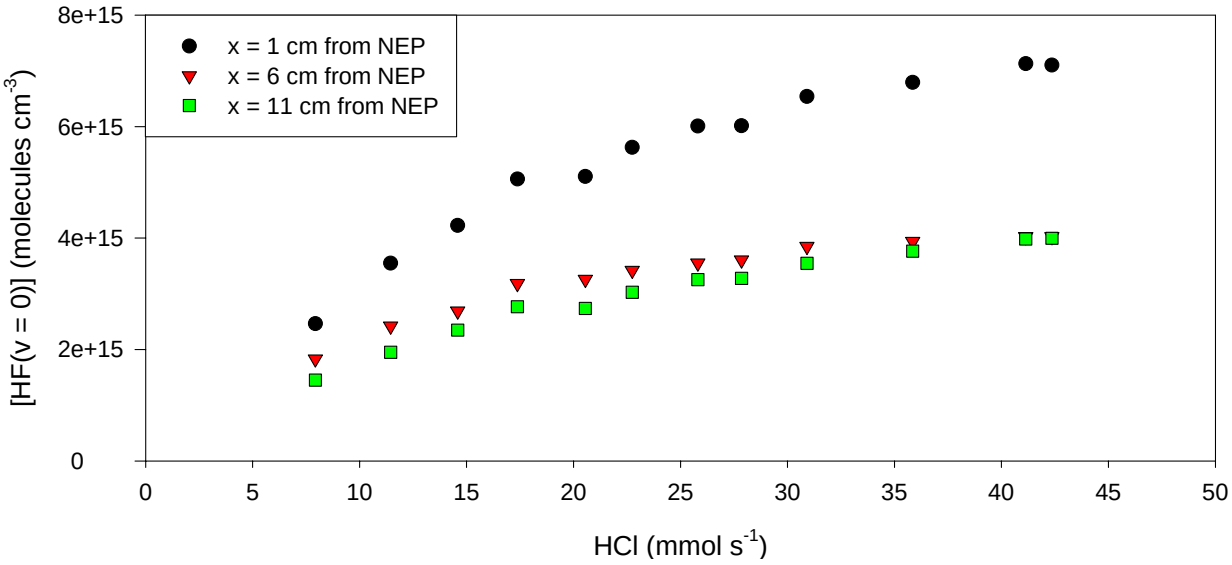

Figure 7. F + HCl titration – Nozzle A/B.

The slow increase to the [HF(v = 0)] beyond HCl = 17 mmol s^{-1} may be a reflection of the very complicated chemistry and kinetics in the combustor and suggests that the addition of HCl may be interfering with the combustion processes. Analysis of the spectral lineshape gives the temperature plot shown in Figure 8.

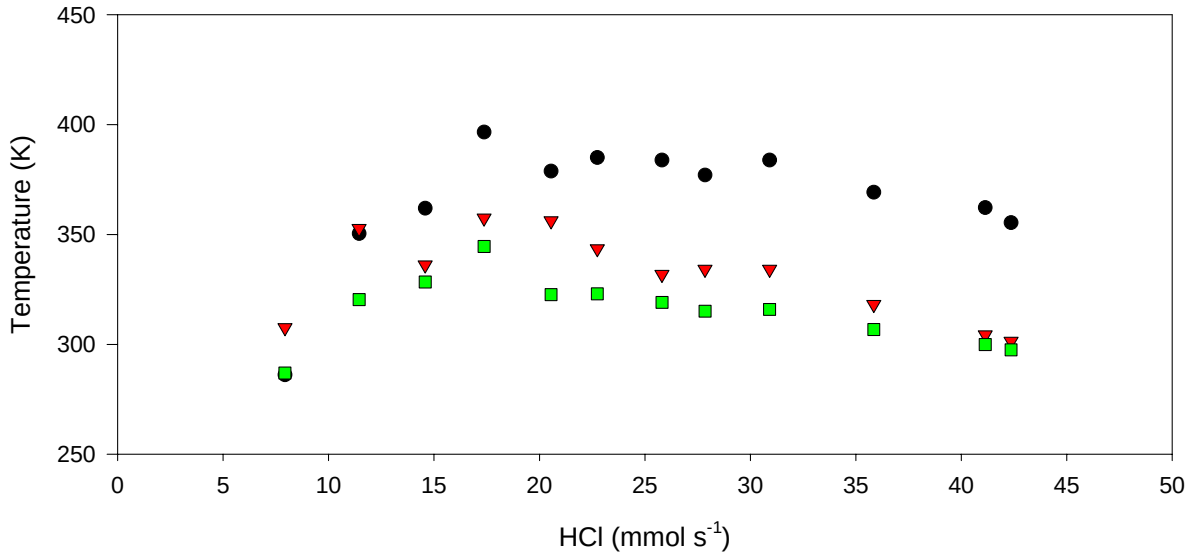

Figure 8. F + HCl titration temperature data – Nozzle A/B

The temperature reaches its maximum at the furthest upstream position and HCl ~ 17 mmol s^{-1}. Further additions of HCl lead to a slow decrease in the temperature, suggesting that the excess HCl is unreacted and acts as a buffer, cooling the combustor flow.

A second titration is shown in the Figure 9 for Nozzle C and F_2 = 10.0, D_2 = 7.5, NF_3 = 0, and He = 10 mmol s^{-1}. In this case, a clear titration end point is observed at HCl = 10 mmol s^{-1}.

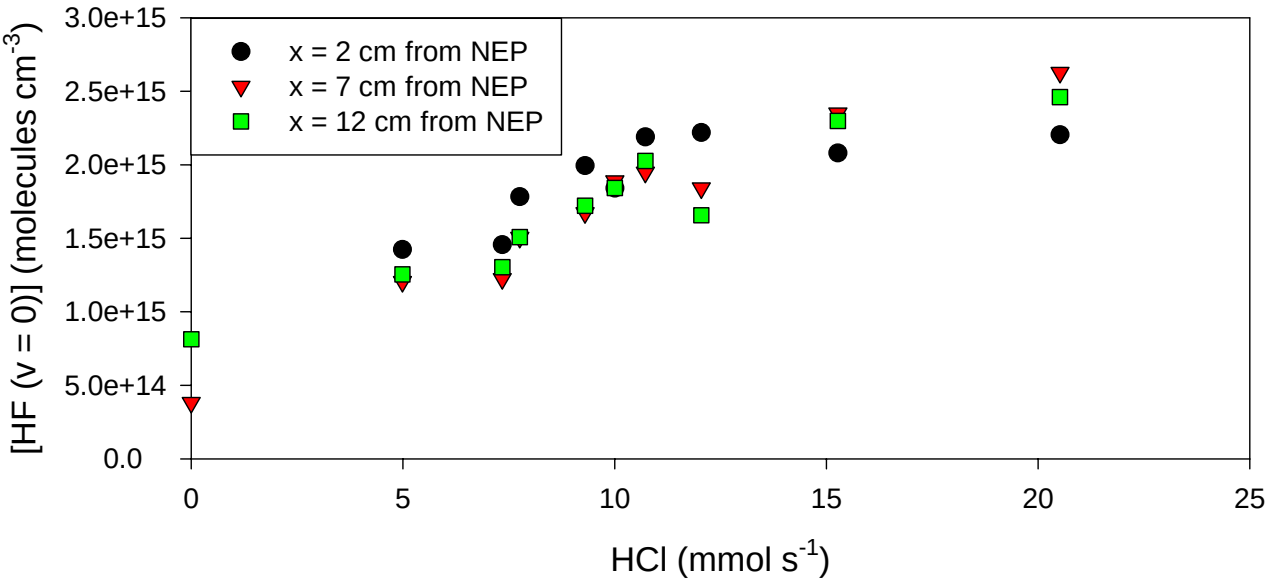

Figure 9. F + HCl titration – Nozzle C

In addition to helping determine the F/Cl atom production efficiency of the combustor, the titrations also provide data necessary to estimate the combustor temperature. The isentropic equation for the ratio between the stagnation and static temperature is

$$\frac{T_0}{T} = \left(1 + \frac{\gamma - 1}{2} M^2\right) \tag{10}$$

where T_0 is the stagnation temperature, and T is the static cavity temperature. As described above, the Mach number is given by the ratio of the stagnation and static pressures and equation (9).

For Nozzles A-B, typical values for P_0 and P are 100 and 1.6 Torr, respectively. Assuming $\gamma \leq 1.667$, equation (9) gives M ~ 3.6 (in the absence of HN_3). This value is slightly larger than the value predicted for the by the nozzle area ratio at the Nozzle Exit Plane (see Table 1) and equation (11):

$$\frac{A}{A^*} = \frac{1}{M}\left[\left(\frac{2}{\gamma + 1}\right)\left(1 + \frac{\gamma - 1}{2} M^2\right)\right]^{\frac{\gamma+1}{2(\gamma-1)}}. \tag{11}$$

This is not surprising because of the large base relief region beyond the NEP; free-jet expansion of the flow leads to higher Mach numbers. According to the titration data, the static temperature is 350 – 400 K for Nozzles A and B, which gives T_0 = 1900 – 2100 K. For Nozzle C, typical stagnation and static (sidewall) pressures are 380 and 6.6 Torr, respectively and equation (9) again gives M ~ 3.6. A stagnation temperature for Nozzle C of 1300 – 1600 K is calculated from equation (10) and the titration data which gives T = 250 – 300 K. Equilibrium calculations for the dissociation of F_2 and NF_3 indicate that these combustor temperatures are consistent with greater than 95% dissociation of F_2 and NF_3.

Emission Spectra

To confirm the presence of NCl($a^1\Delta$), NCl($b^1\Sigma^+$), and I*($^2P_{1/2}$), a series of emission spectra were collected, see Figures 10 - 12. The spectrum shown in Figure 10 was collected with the OMA V camera and clearly indicates the presence of these species and the absence of any strong extraneous emissions. A second, unsaturated, NIR spectrum is shown in Figure 11. A visible emission spectrum, collected with a CCD is shown in Figure 12. It is important to note that the visible portion of the spectrum shown in Figure 10 is weak because the OMA V instrument has a poor response at 665 nm.

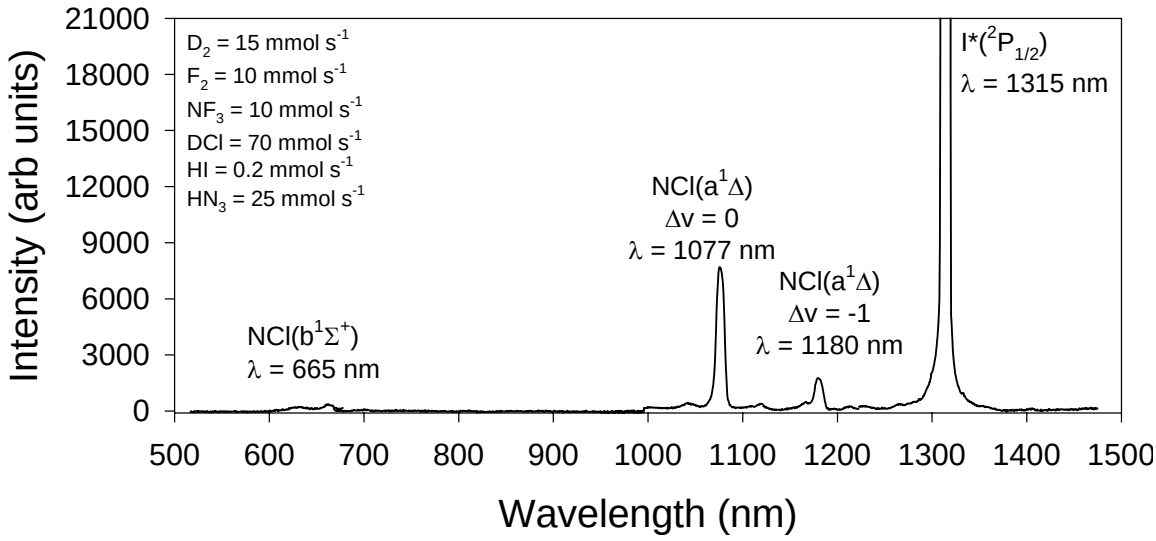

Figure 10. NIR Emission Spectrum - I*($^2P_{1/2}$) saturated.

For all three spectra the experimental conditions were F_2 = 10, D_2 = 15, NF_3 = 10, DCl = 70, HI = 0.2, and HN_3 = 25 mmol s^{-1}. The I*($^2P_{1/2}$) signal is quite strong and saturates the camera at the resolution (i.e. slit width) used for Figure 10. A spectrum collected at a slit width that does not saturate the detector is shown in Figure 11 below:

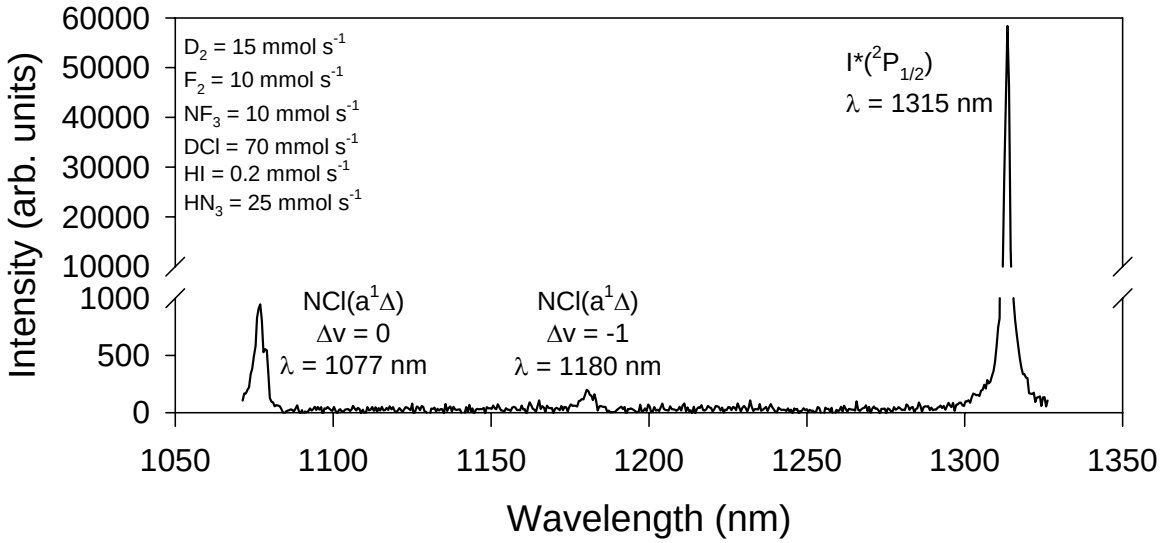

Figure 11. NIR Emission Spectra – unsaturated.

Under these experimental conditions the ratio of the I*($^2P_{1/2}$) and NCl($a^1\Delta$) spectral areas is approximately 60 : 1. The radiative lifetimes[36-38] for NCl($a^1\Delta$) and I*($^2P_{1/2}$) are 2.7 and 0.2 s, respectively, and the detector response function across the wavelength region shown is constant. Hence, this ratio corresponds to a NCl($a^1\Delta$) : I*($^2P_{1/2}$) density ratio of 0.23. While the very intense I*($^2P_{1/2}$) emission is encouraging, the low [NCl($a^1\Delta$)] : [I*($^2P_{1/2}$)] ratio could be problematic – especially for an energy transfer laser where the energy carrier density should far exceed the density of the lasing species. Spectra collected in the absence of HN_3 show weak, transient signals at 1050, 1200, and 1300 nm. The 1300 nm signal is readily assigned to HF(Δv = 2) emission, but the other features are not immediately identifiable. The transient nature of the emissions (they disappear after a few seconds) and the simultaneous appearance of HF overtone emission suggest that they are related to the combustion process, possibly NF* or NF_2*.

A visible emission spectrum is shown in Figure 12.

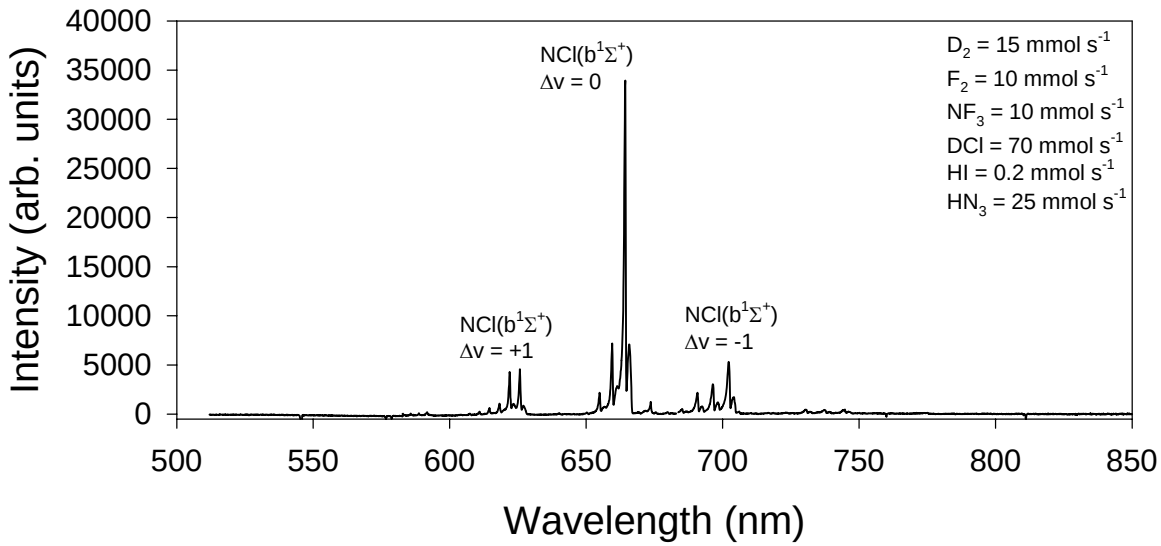

Figure 12. Visible Emission Spectrum

The conditions are identical to those used in Figures 10 and 11. The only obvious emissions are readily assigned to NCl($b^1\Sigma^+ - X^3\Sigma^-$), $\Delta v = 0, \pm 1$. The weaker bands at 600 - 625 and 675 - 715 nm indicate the presence of vibrationally excited NCl($b^1\Sigma^+$). In addition, the very weak emissions at ~575 and ~740 nm are consistent with $\Delta v = \pm 2$ emissions, further evidence supporting the presence of NCl($b^1\Sigma^+$, $v > 0$).

Small signal gain spectra

As demonstrated in the preceding section, addition of HN_3 to the combustor products generated $NCl(a^1\Delta)$ and $I^*(^2P_{1/2})$. Under a variety of conditions, we observed positive small signal gain, see Figures 13 and 14.

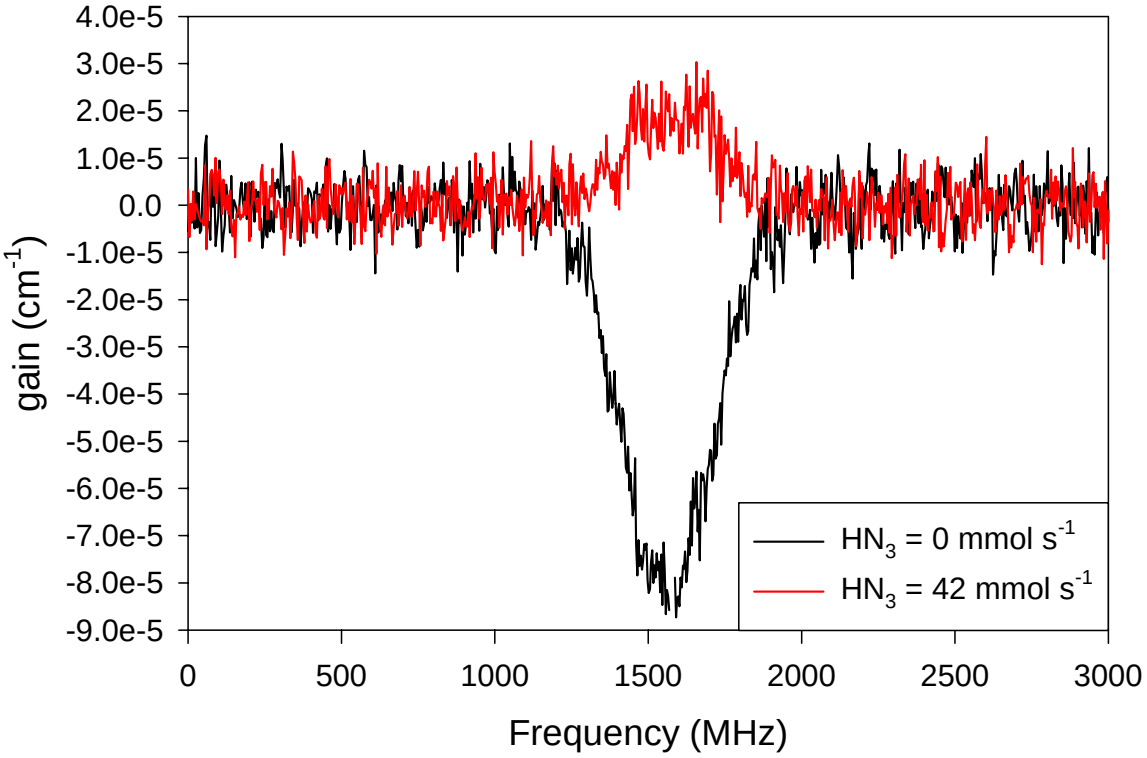

Figure 13. Initial gain demonstration.

The first ever demonstration of gain in a supersonic reactor based on the AGIL concept is shown in Figure 13. The conditions were F_2 = 10, D_2 = 7.5, NF_3 = 22, DCl = 50, HI = 0.25, and He(primary) = 210 mmol s^{-1}. Nozzle B was used and the cavity pressure increased from 6.8 to 9.8 Torr upon addition of 42 mmol s^{-1} of HN_3 and 381 mmol s^{-1} of He. As the data shows, the small iodine absorption signal is converted to positive gain upon the addition of HN_3. The positive gain was observed at x = 11 cm from the nozzle exit plane (NEP); the signals at x = 1 and 6 cm, on the other hand, exhibited optical transparency.

Numerous demonstrations of positive gain were achieved – a set of spectra collected under the optimum conditions of Nozzle C are shown in Figure 14:

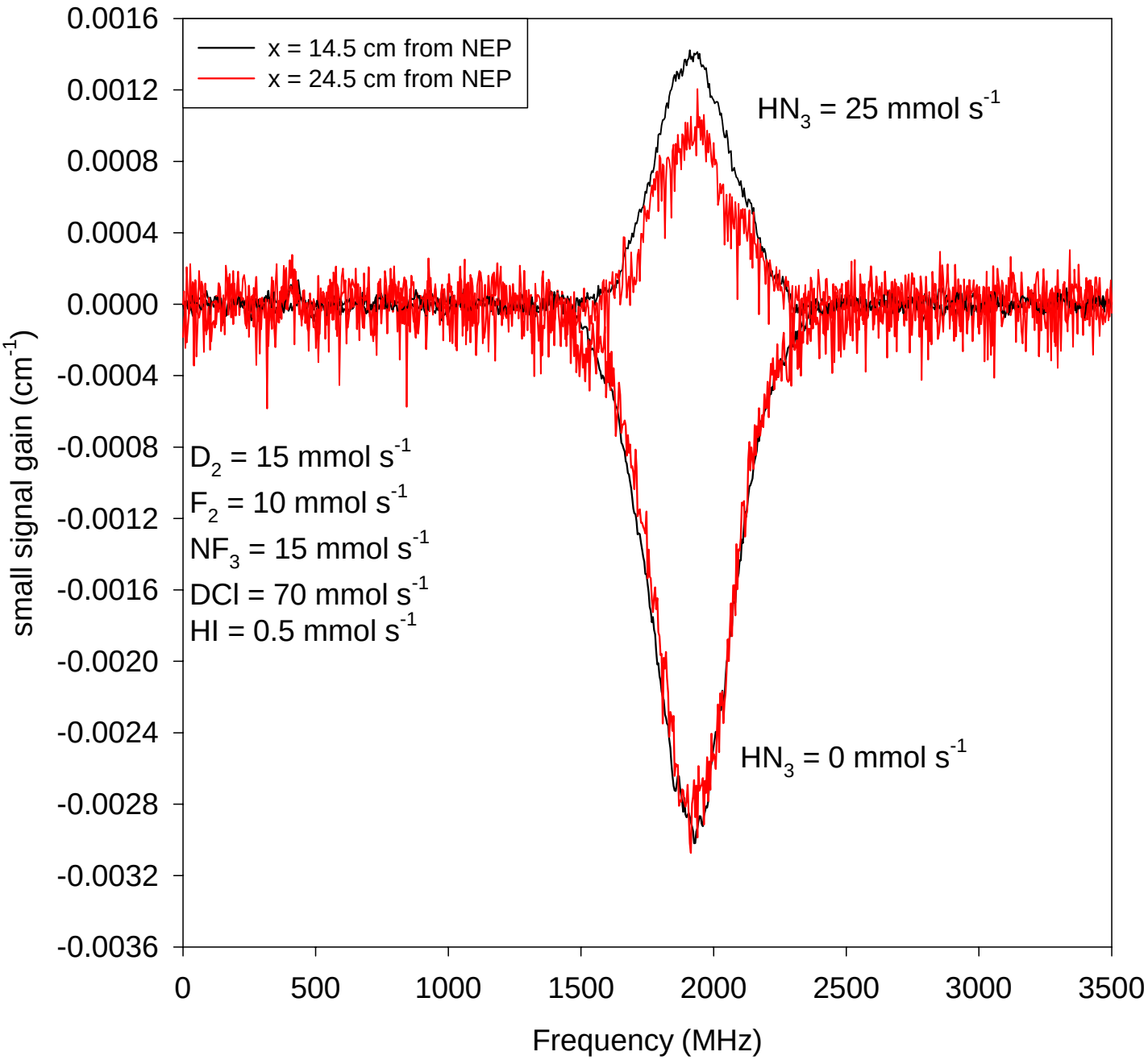

Figure 14. Optimized gain spectra.

Small signal gain optimization

Dependence on combustion reagents

Experimental series were performed to optimize the small signal gain as a function of the starting conditions. The data are shown in Figures 15 – 25 below. Unless noted otherwise, the data were generated using Nozzle C.

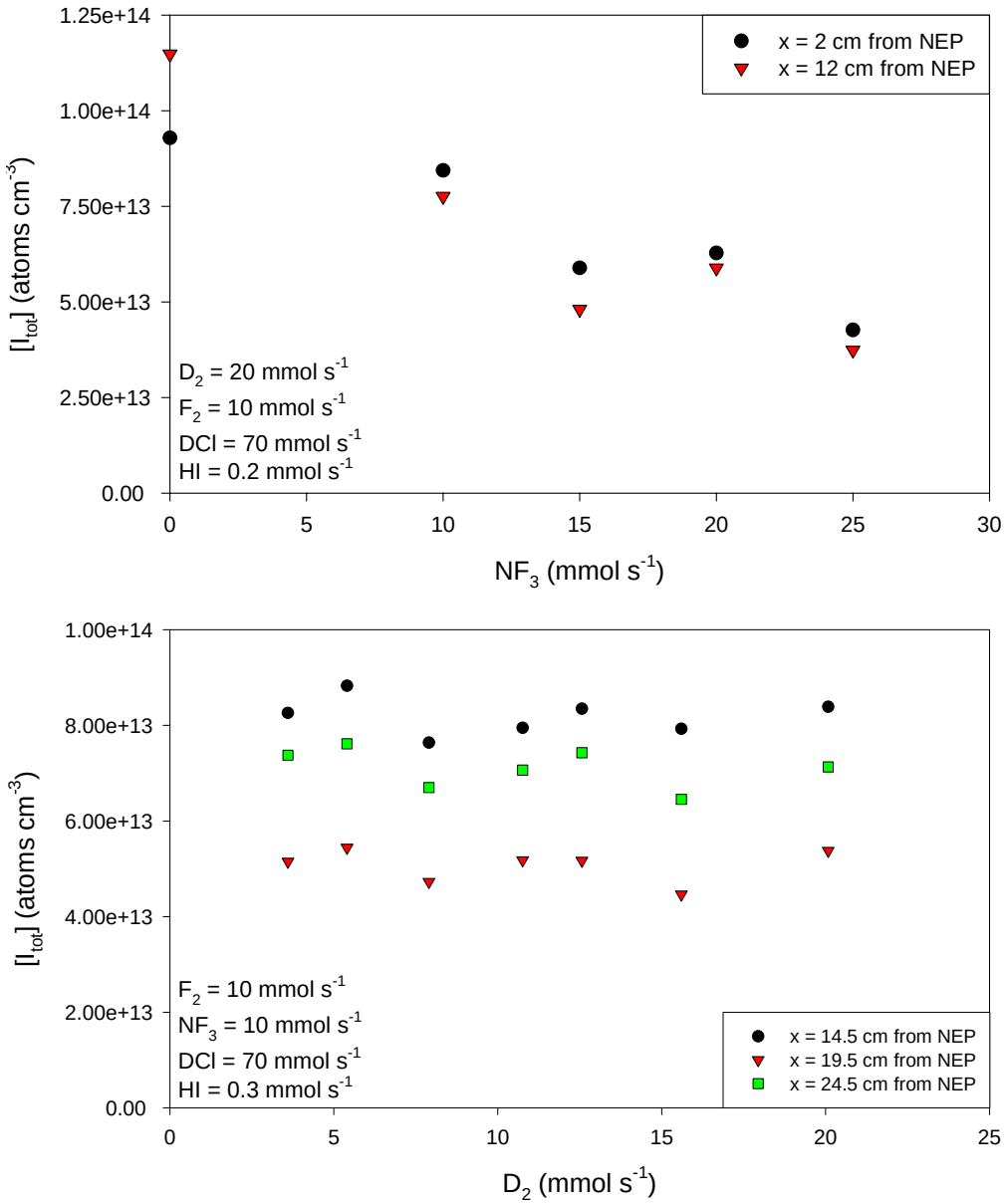

Figure 15. $[I_{tot}]$ vs. NF_3, and D_2.

The upper and lower panels of Figure 15 show [I_{tot}] plotted as a function of NF_3 and D_2. This test was performed because the addition of NF_3 and D_2 tend to change the performance of the combustor. Variation of the molecular fluorine flow rate would have also changed the combustor performance. However, for the sake of safety and simplicity, the F_2 flow was fixed at the highest flow rate that could be safely sustained by the device and hardware. Because variable combustor performance was possible, the total amount of iodine atoms, [I_{tot}], could also vary significantly. As the upper panel of Figure 15 shows, the addition of excess NF_3 tends to reduce the density of iodine atoms generated by the combustor. Since the iodine atom flow rate is a very minor component to the total flow, the reduction is not likely caused by a reduction of the number of Cl and/or F atoms produced by the combustor. Although 95% or more of the NF_3 is fully dissociated, this reduction may be the result of reactions between NF_x and I. The more likely scenarios are I atom recombinations catalyzed by one or more products of the combustor, or another unknown mechanism that chemically consumes I atoms. Whatever the cause, the clear result is reduced [I_{tot}].

The lower panel of Figure 15, on the other hand, conclusively demonstrates that varying D_2 flow rates do not lead to significant changes to [I_{tot}]. Considering that D_2 does not react well with I_2 or I, this is not a surprising result.

Figure 16 demonstrates the change in the combustor temperature as a function of NF_3 variation. The combustor conditions are as indicated in the plot. The cavity temperature increases slightly as the flow progresses downstream. In addition, the temperature increases with added NF_3 up to NF_3 = 20 mmol s^{-1}. A slight decrease in temperature beyond NF_3 = 20 mmol s^{-1} is apparent, but the difference is well within the margin of error (± 10%) for this type of measurement.

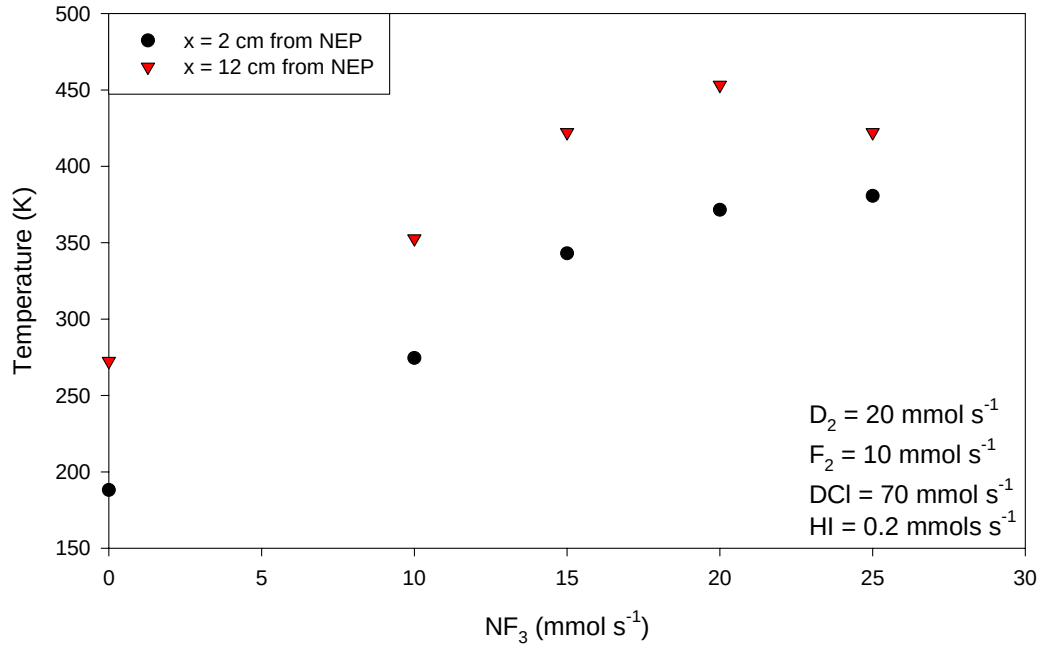

Figure 16. Cavity temperature vs. NF_3 prior to HN_3 injection.

The corresponding temperature plot for varying D_2 is shown in Figure 17.

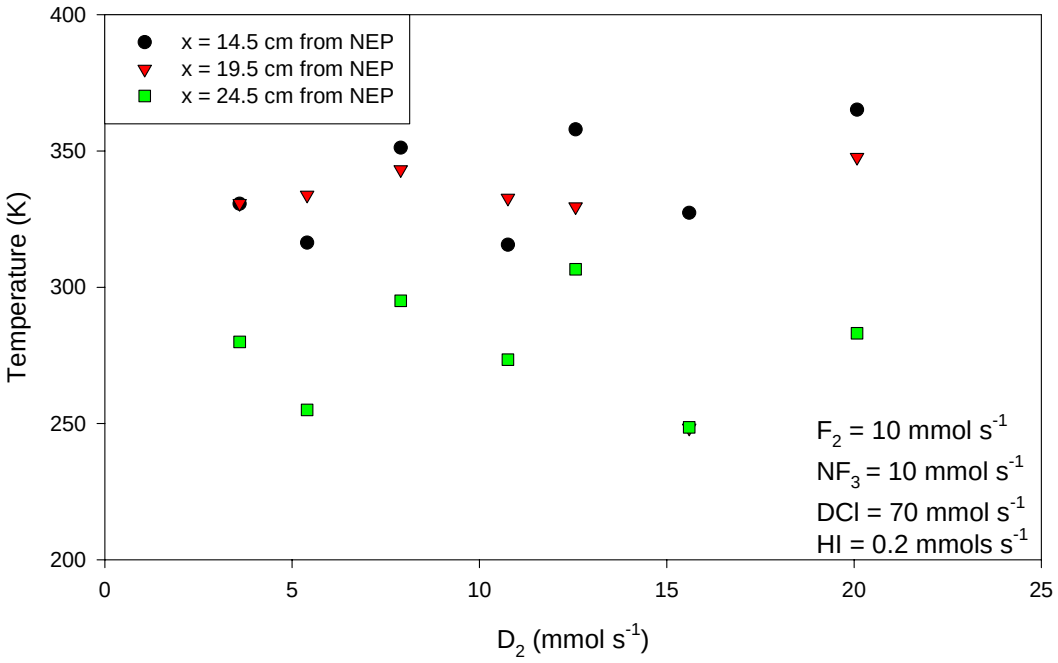

Figure 17. Cavity temperature vs. D_2 prior to HN_3 injection.

These data were collected further downstream than the NF_3 data shown in Figure 17; as a result, the highest temperatures are observed at the furthest upstream position and the temperature

decreases as the flow progresses downstream. There does not appear to be a systematic variation in the temperature as a function of D_2 added to the combustor. This is a somewhat surprising result since D_2 should react with the large bath of F atoms that are present in the combustor and increase both the combustor and cavity temperatures.

Figure 15 demonstrates that variations of the combustor conditions can lead to variations in the total I atom density, even for constant and small [HI]. In an effort to normalize out the variability of $[I_{tot}]$, % inversion is plotted as a function of the starting conditions in addition to the small signal gain. The % inversion is defined as

$$\%\ inversion = \frac{\left[I^*(^2P_{1/2})\right]}{\left[I_{tot}\right]} * 100\% \qquad (12)$$

and inversion > 33% indicates positive gain.

As Figures 18 – 25 show, positive gain was observed over a wide range of conditions and for a relatively long distance along the flow reactor. Figures 18 – 25 indicate that in almost all cases optical transparency (i.e. gain = 0) was observed at the x = 19.5 cm position even though positive gain was observed in some instances at both x = 14.5 and 24.5 cm. The x = 19.5 position in the flow probably has positive gain as well, but not enough to be distinguished from the detector noise.

Figure 18 shows that the gain is strongly dependent on the NF_3 flow rate, but only weakly dependent on D_2. Large fluences of NF_3 lead to a decrease in the % inversion and the small signal gain most likely because of the reactions that suppressed $[I_{tot}]$ in Figure 15 above. The gain and % inversion increase for D_2 = 2.5 = 7.5. Further additions of D_2 do not appear to have any systematic effect on % inversion or gain.

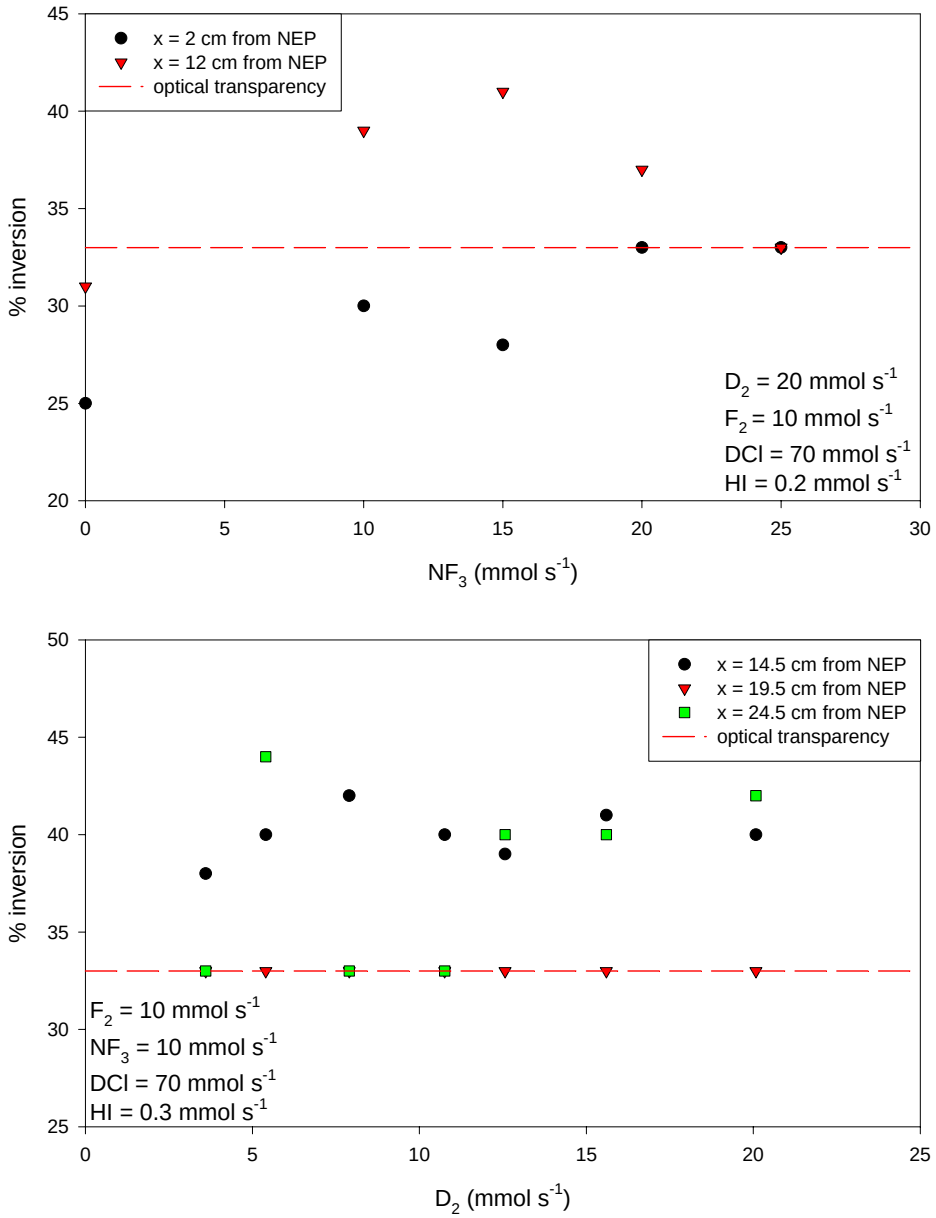

Figure 18. % inversion vs. NF_3 and D_2.

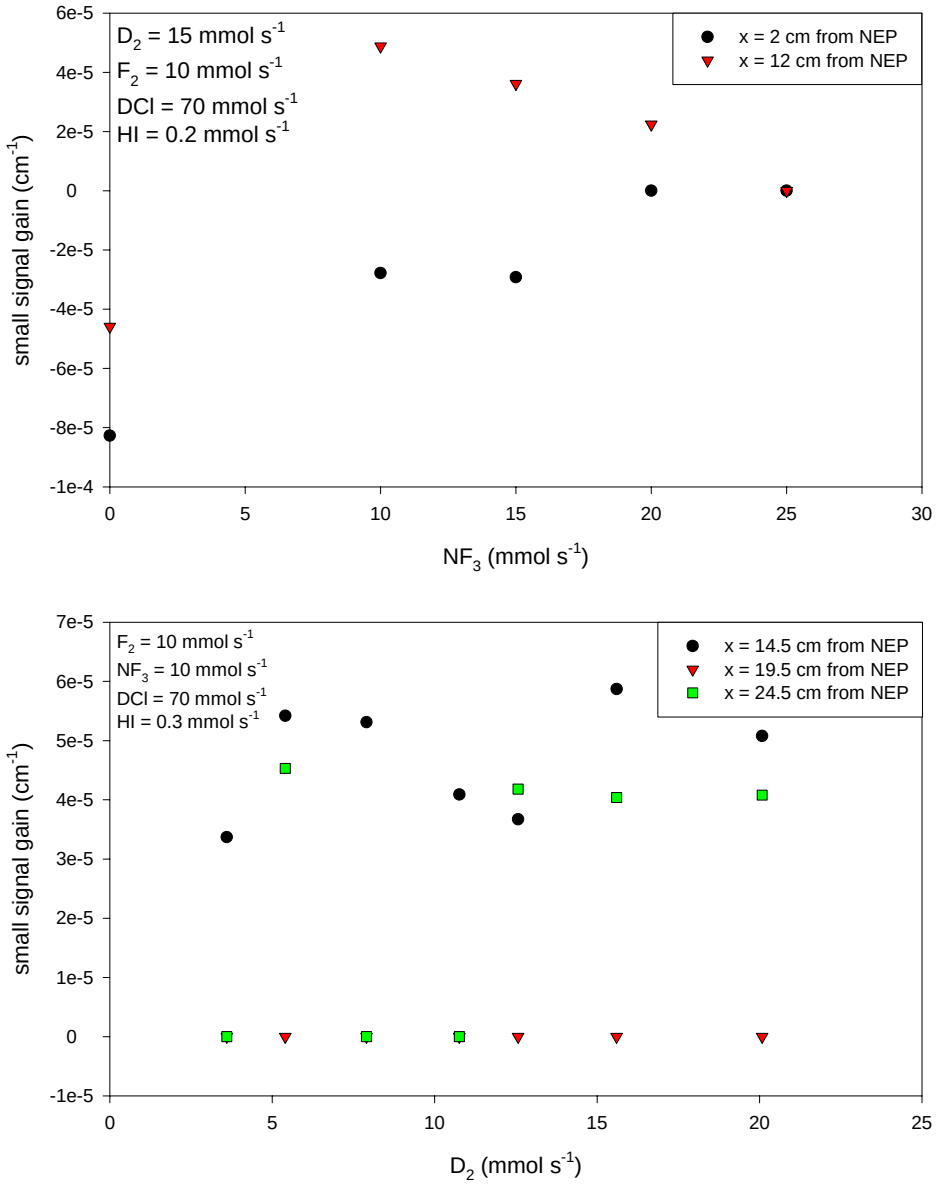

Figure 19. Small signal gain vs. NF_3 and D_2.

Experimental series exploring the dependence of $[I_{tot}]$, temperature, and gain on the DCl flow rate were performed but are now shown here because the data is unremarkable. The DCl flow does not interfere to any significant extent with the combustion products. Moreover, because the generation of $NF(a^1\Delta)$ is highly undesirable, DCl was always added in sufficient excess to ensure that all F atoms generated by the $D_2/F_2/NF_3$ combustion process were converted to Cl atoms.

Dependence on HN_3 and HI

The two most critical flows for generating gain on the $I^*(^2P_{1/2}) - I(^2P_{3/2})$ transition are the HI and HN_3 flows. Figures 20 and 21 show the relationship between % inversion and small signal gain, respectively, vs. the HN_3 flow rate. The experimental conditions for both plots are F_2 = 10, D_2 = 15, NF_3 = 15, HI = 0.3, DCl = 70, and He(primary) = 110 mmol s^{-1}.

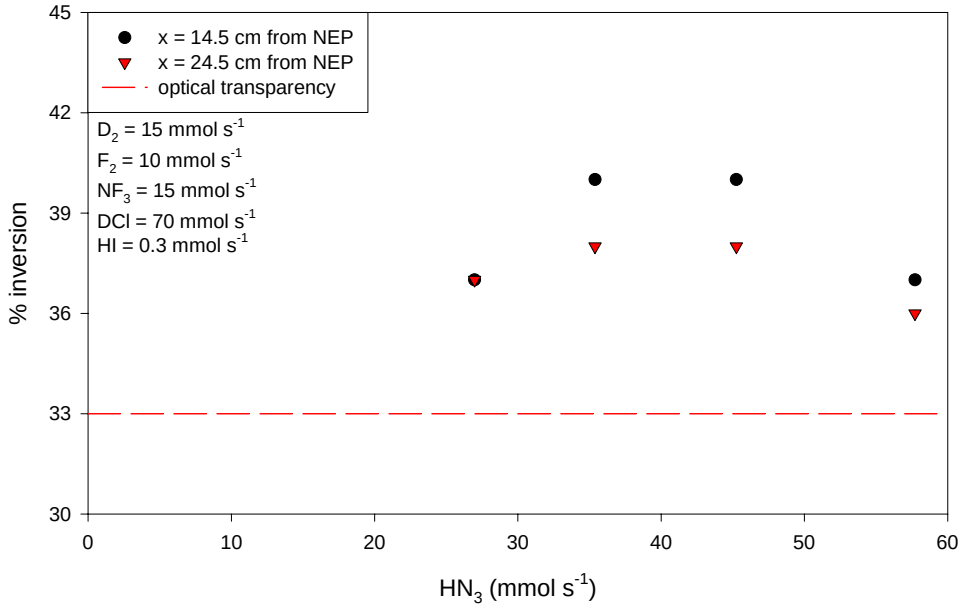

Figure 20. % inversion vs. HN_3.

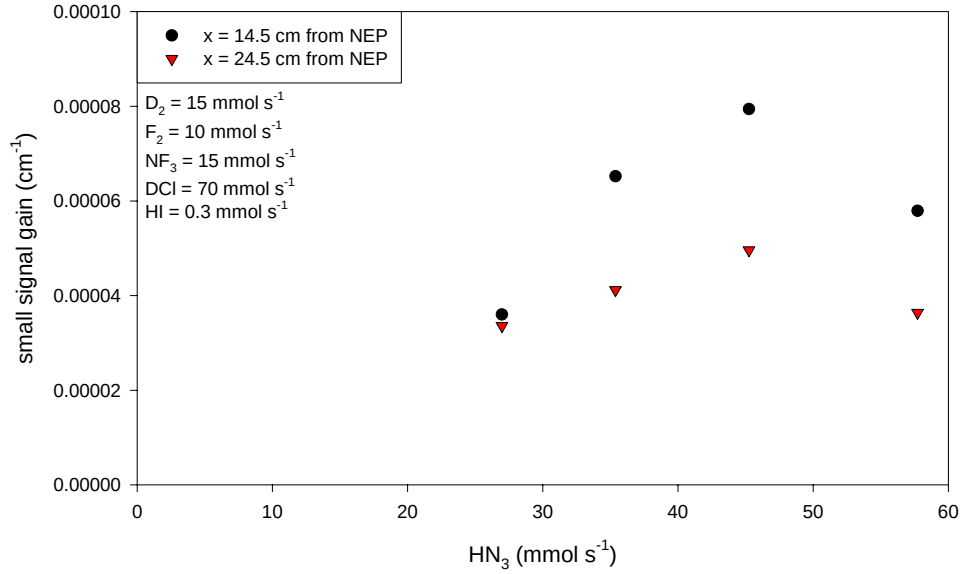

Figure 21. Small signal gain vs. HN_3

The relationship between gain and HN_3 is an important indicator of the overall efficiency of AGIL chemistry; if the HN_3 flow rate greatly exceeds the estimated Cl atom flow rate (or vice-versa) this would constitute evidence for poor $HN_3 \rightarrow NCl(a^1\Delta)$ conversion and/or poor mixing. The data in Figure 20 indicate an optimum inversion for $HN_3 \sim 45$ mmol s^{-1}. Titrations for these conditions give Cl ~ 40 mmol s^{-1} and the experimentally optimum Cl : HN_3 ratio is 0.89. Since each $NCl(a^1\Delta)$ molecule requires 2 Cl atoms to produce, stoichiometry states that the Cl : HN_3 ratio should be 2. While the Cl : HN_3 ratio for this device does not match the stoichiometric value, it is a significant improvement over the optimum values measured in the subsonic AGIL experiments; AGIL 1 and AGIL 2 had Cl : HN_3 ratios of 0.25 and 0.40, respectively. The highest small signal gain shown in Figure 21 is 7.94×10^{-4} cm^{-1}.

Plots of % inversion and small signal gain vs. HI are shown in the upper and lower panels of Figure 22, respectively. The experimental conditions were F_2 =10, D_2 = 15, NF_3 = 15, DCl = 70, He(primary) = 110, and HN_3 = 25 mmol s^{-1}. The data clearly show that the inversion and gain decrease with added HI. Since HI is added upstream of the nozzle where F and Cl atoms are the main species, the HI is rapidly converted to iodine atoms. The decreasing gain is consistent with rapid depletion of $[NCl(a^1\Delta)]$ by iodine atoms via energy transfer.

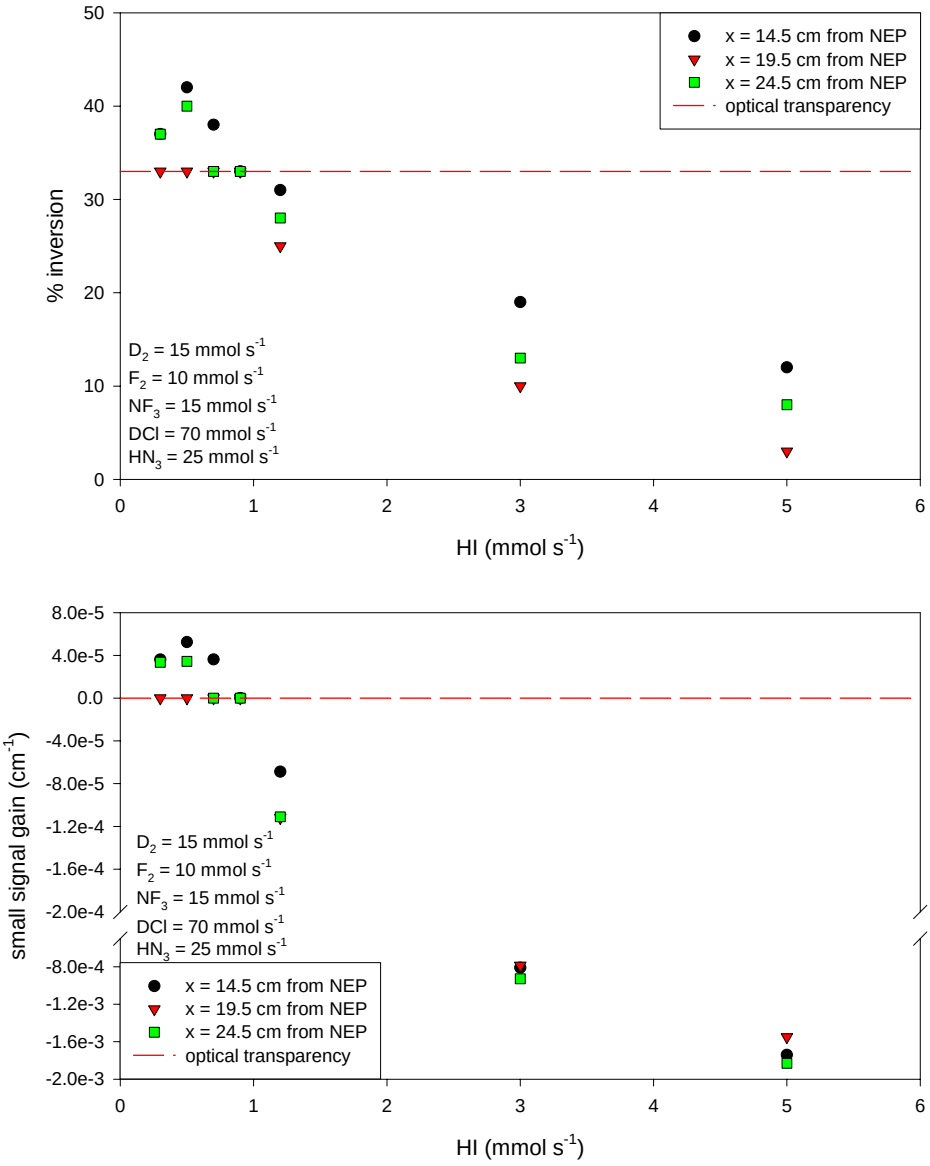

Figure 22 % inversion and small signal gain vs. HI.

Dependence on secondary flows

In addition to the gain optimization wth respect to the reactive chemistry, experimental series that examined the effect of secondary flows were also performed. In most cases, the addition of He to the reactor had little or no effect on [I_{tot}], temperature, or small signal gain over a modest range of flow rates. The tunnel purge flow rate, on the other hand, did affect the main flow in a rather surprising manner. Figure 23 shows the dependence of the spectroscopically determined temperature as a function of the tunnel purge He.

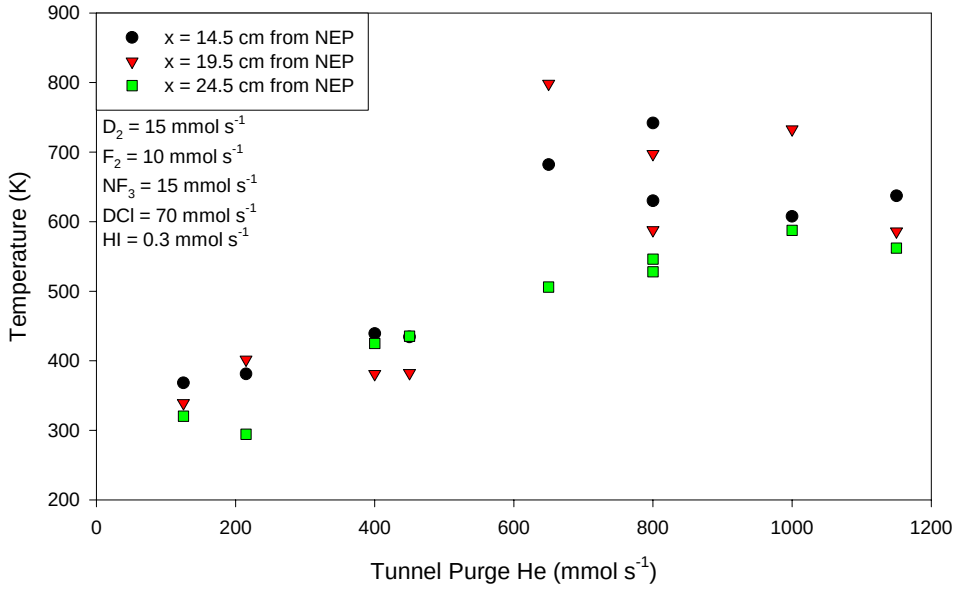

Figure 23. Cavity temperature vs. Tunnel Purge He.

Although there is some scatter at He(tunnel) = 800 – 1000 mmol s^{-1}, the overall trend indicates an increase in the temperature as the He flow is increased. It is important to note that the data points shown in this figure were collected over the course of two separate experimental series and on different days. Though it is not shown, a slight concomitant increase in the cavity pressure was also noted as the tunnel purge flow was increased. However, the [I_{tot}] was effectively constant for the entire span of He(tunnel).

Figure 24 shows the dependence of the measured % inversion as a function of He(tunnel). Two obvious trends can be discerned from the data. First, the % inversion decreases as the flow progresses downstream. (When combined with similar data at x = 2 – 12 cm, it is clear that the peak gain is found between x = 12 – 14 cm.) More importantly, however, is the clear enhancement to the small signal gain as the He tunnel purge flow is increased. Clearly, He(tunnel) is an important parameter for optimizing the small signal gain.

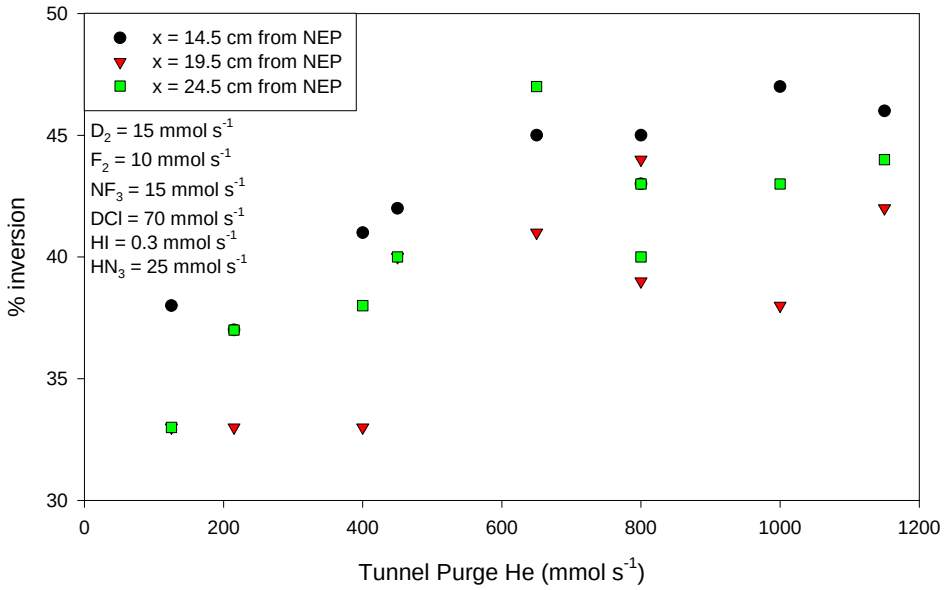

Figure 24. % inversion vs. Tunnel Purge He

The corresponding plot of small signal gain vs. tunnel purge He is shown in Figure 25.

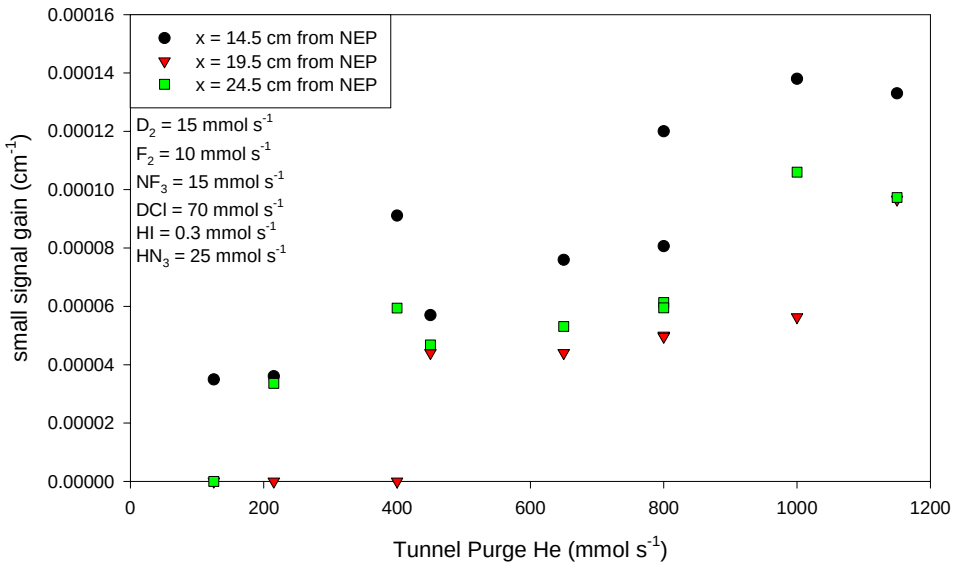

Figure 25. Small signal gain vs. Tunnel Purge He.

Consistent with the % inversion data in Figure 24, the highest gain is observed at He(tunnel) = 1000 mmol s^{-1}.

Vertical profiles of % inversion and gain

Vertical profiles of [I_{tot}] and temperature were shown above in Figures 4 – 6. Corresponding plots of % inversion and small signal gain (following the addition of HN_3 = 25 mmol s^{-1}) for the conditions of Figure 6 are shown in Figure 26. Interestingly, the gain persists for ±5 mm beyond the vertical centerline and optical transparency persists another ± 5 mm. The actual nozzle half-height at the nozzle exit plane is 4 mm from the centerline; expansion of the flow into the base purge region is evident but does not appear to be a major problem.

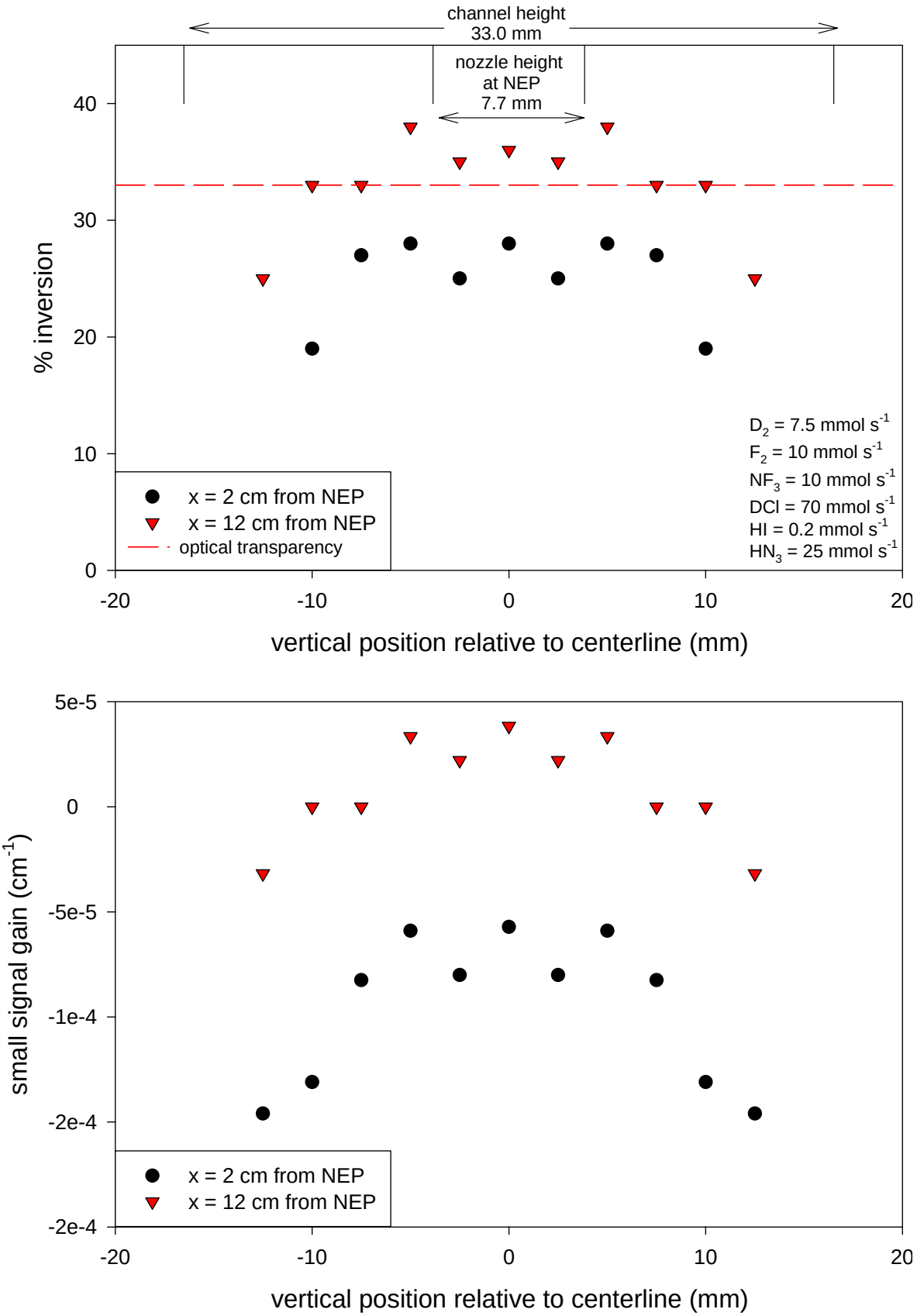

Figure 26. Vertical profile of % inversion and small signal gain

Adding HN_3 to the combustor

A single series of experiments were performed with the Nozzle D configuration. As described above, Nozzle D allowed HN_3 injection into the high-temperature, high-pressure regime of the combustion chamber. The expectations going into this series of tests were that if the large excess of He that accompanied the HN_3 did not extinguish the combustor, then the HN_3 would likely thermally dissociate before it could react to any significant extent with Cl atoms.

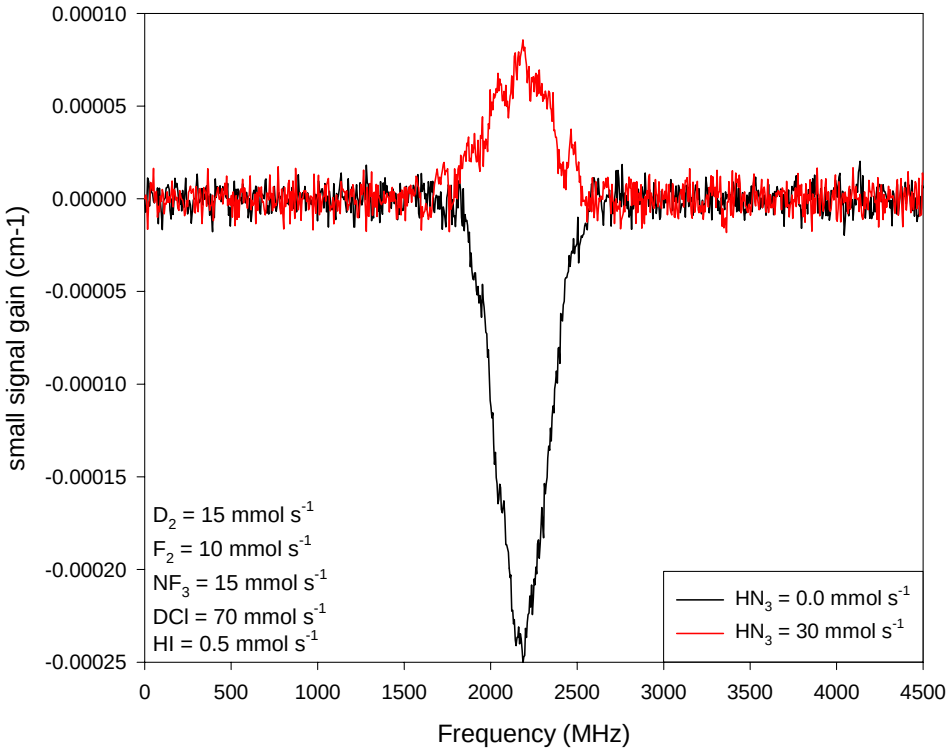

Figure 27. Gain demonstration – Nozzle D.

Interestingly, these expectations turned out to be completely unfounded. The combustor did not extinguish upon the addition of 10% HN_3, and small signal gain was reproducibly observed at x = 11.5 cm downstream of the NEP. Figure 27 shows an example gain demonstration. While the gain was quite low ($g = 6.8 \times 10^{-5}$ cm^{-1}) and the inversion was observed for a relatively narrow range of conditions, the observation of gain at all is a significant and important result.

Attempts to detect NCl($X^3\Sigma^-$)

The NCl($X^3\Sigma^-$) diagnostic uses a ratiometric detection scheme to eliminate noise associated with fluctuations of the laser intensity. This enables very low absorption signals to be measured[35]; calibrations performed at PSI with molecular I_2 found that absorptions as low as 10^{-4} could be measured by this instrument with a reasonable signal to noise ratio. Given the NCl($X^3\Sigma^-$) – NCl($b^1\Sigma^+$) absorption line strength factor of 1.53 x 10^{-19} cm molecule^{-1} and a single pass path length of 5 cm, an easily observable absorption of ~3.5 x 10^{-3} should be produced by [NCl($X^3\Sigma^-$)] = 1 x 10^{14} cm^{-3}.

Figure 27 shows sample absorption spectra measured for D_2 = 7.5, F_2 = 10, NF_3 = 20, DCl = 70, and HI = 0.2 mmol s^{-1}. The diode laser probed a region ~ 7 cm downstream of the

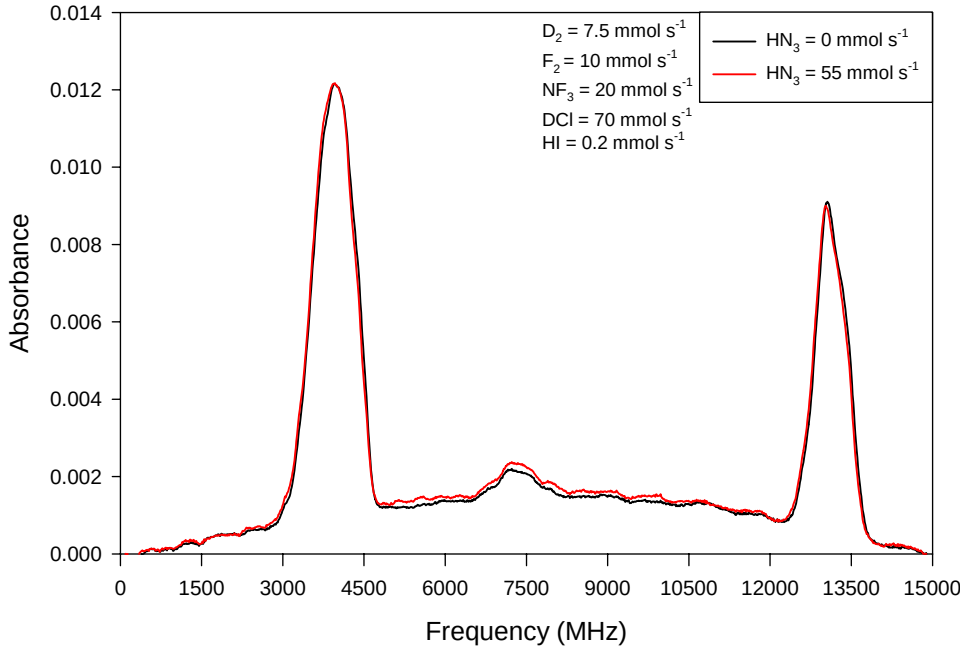

Figure 28. Attempt to measure NCl($X^3\Sigma^-$).

NEP. A 10 cm cold iodine cell was placed between the reactor and diode laser as a reference. The two traces show the spectrum with and without HN_3 = 55 mmol s^{-1} added to the reactor.

The I_2(5,6) R(51) and P(44) lines (often referred to as lines 122 and 123, according to the I_2 spectroscopic atlas of Gerstenkorn and Luc[39]) are easily observed with a high signal to noise ratio, but the NCl($X^3\Sigma^-$) absorption signal that should appear between these two peaks is absent. Additional attempts were made for a variety of conditions including excess HI and at x = 12 cm from the NEP. In principle, excess HI should generate a sufficient density of I atoms to quench all of the NCl($a^1\Delta$) to NCl($X^3\Sigma^-$). In all cases, no absorptions that could be attributed to NCl($X^3\Sigma^-$) were observed.

An estimate for the density of NCl($X^3\Sigma^-$) in our device can be made using the data from the small signal gain measurements. According to equation (1), each I*($^2P_{1/2}$) atom is accompanied by the generation of an NCl($X^3\Sigma^-$) molecule. Given a typical $[I_{tot}] \leq 1 \times 10^{14}$ cm^{-3} and optimum gain of 1×10^{-4} cm^{-1} (i.e. inversion ≤ 45%), $[I^*(^2P_{1/2})] = [NCl(X^3\Sigma^-)] \leq 4.5 \times 10^{13}$ cm^{-3} is calculated. This value will be larger if significant amounts of NCl($X^3\Sigma^-$) is generated by additional collisional quenching or directly by reaction (5). It will be lower, on the other hand, if the energy transfer or other quenching reactions produce significant quantities of NCl($X^3\Sigma^-$, $v \neq 0$) or if there are rapid reactions which consume NCl($X^3\Sigma^-$). Ground state NCl densities on the order of $4 – 5 \times 10^{13}$ cm^{-3} should be sufficient to generate a resolvable absorption signal, albeit rather weakly.

Given this estimate, it is surprising that the attempts to measure NCl($X^3\Sigma^-$) under the operating conditions of Nozzles A – C showed no evidence of absorption. The lack of an observable signal is puzzling and suggests that NCl($X^3\Sigma^-$, v = 0) is a very minor component of the flow or that NCl($X^3\Sigma^-$) is eliminated by chemical reaction on a very fast time scale.

Discussion and Conclusions

There are multiple conclusions and trends evident from these data and experiments. The first is that the AGIL chemistry is robust: quantities of $NCl(a^1\Delta)$ and small signal gain values sufficient for lasing can be generated using technology that has been proven to be scalable by the HF laser community[40]. In particular, we have proven that a high temperature chemical combustor can be used as a source of Cl atoms and that small signal gain can be generated upon supersonic expansion and the addition of HN_3 and HI. The results from Nozzle D further underscore the resilience of the AGIL chemistry.

One particularly surprising result was the dependence of the gain on the He(tunnel) flow rate. There are at least two possible explanations for this behavior. First, the increased purge flows may be compressing the flow along the direction of the optical axis. This would lead to slightly higher densities and slightly higher temperatures – both of which can lead to faster and more efficient $NCl(a^1\Delta)$ production. However, plots of $[I_{tot}]$ vs. He(tunnel) (not shown) demonstrate no systematic variation. Furthermore, visual observation of the flow does not indicate any significant compression of the flow along the optical axis. The second explanation involves the possibility of shocks generated by the extra He flow in the downstream portion of the flow reactor. This would lead to a slower flow and a lower Mach number. Whatever the exact mechanism is, the data strongly suggest that even better performance may be achieved by building a supersonic nozzle with a lower A/A* ratio and Mach number.

In addition, this work has identified where the focus of future work should be placed in order to enable and demonstrate a high-energy (i.e. multi-kW) laser system. Specifically, the future utility of AGIL depends on designing a nozzle that creates the optimal reaction conditions in the supersonic flow region but also allows efficient mixing of the HN_3 fuel. Nozzles A & B,

for example, produced a supersonic flow with T = 400 – 500 K. According to temperature-dependent rate constant measurements and the previous subsonic AGIL work[1, 24], this is nearly optimal for $NCl(a^1\Delta)$ formation. Unfortunately, Nozzles A-B gave rather poor penetration and mixing of HN_3. Inspections of the visible chemiluminescence showed two bright red flames that began at the HN_3 injectors and extended beyond the observation region downstream. The vertical centerline of the reactor remained dark, indicating the absence of $NCl(b^1\Sigma^+)$ (and, by inference, $NCl(a^1\Delta)$) for all but the highest HN_3 flow rates. On the other hand, full penetration of the HN_3 into the main flow was achieved with the smaller throat height and shallower expansion angle Nozzle C, but in this case the initial temperature was only ~250K – too low for fast, efficient generation of $NCl(a^1\Delta)$. It is clear that future generations of AGIL technology must pay careful attention to the details of the supersonic nozzle in order to optimize the generation rate of $NCl(a^1\Delta)$.

A second challenge for future AGIL devices is tied to the laser fuel, HN_3. Because of its potential (some would say propensity) for explosive decomposition, the storage and dynamic pressure of HN_3 must be kept low. For example, while the vapor pressure for HN_3 at room temperature is nearly 400 Torr, safety concerns limit the practical storage partial pressure to only 100 – 200 Torr. Since the degree of penetration depends upon the pressure difference between the plenum pressure of the injected fluid and the static pressure of the main flow, the HN_3 must be highly diluted in order to get the plenum pressure to an acceptable level. Unfortunately, the addition of large flows to the supersonic fluid can lead to shocks or even unchoke the supersonic nozzle. Just as importantly, the need for low pressure storage of HN_3 leads to highly inefficient storage systems. In our case, the HN_3 is stored in six 150 L tanks. These tanks consume a significant amount of laboratory space, take 3 – 4 days to fill, and are only sufficient for a single

day of experiments. Clearly, future generations of AGIL technology must incorporate a more compact, efficient, and sustainable HN_3 generation and delivery system.

Despite these important challenges, we consider this work to be a complete success and a major breakthrough in chemical laser technology. In fact, supersonic AGIL is the first fully chemically driven chemical laser system since the invention of COIL in 1978, over 26 years ago. In principle, AGIL has the potential to be significantly more weight efficient than COIL because AGIL uses all gas-phase reagents. Moreover, because AGIL incorporates the same chemical combustor technology used by the HF/DF laser community, many of the issues related to building a large-scale combustion-driven laser have already been addressed, and/or solved. Thus, assuming that the issues related to safety of using high fluences of hydrogen azide can be overcome, the rapid development of high-energy AGIL devices should be forthcoming.

References

[1] G. C. Manke II, C. B. Cooper, S. C. Dass, T. J. Madden, and G. D. Hager, "A Multi-Watt All Gas-phase Iodine Laser (AGIL)," *IEEE J. Quant. Elect.*, vol. 39(8), pp. 995 - 1002, 2003.

[2] G. C. Manke II, T. L. Henshaw, Chris B. Cooper, and G. D. Hager, "Recent Progress in the Development of a Multi-Watt All Gas-Phase Iodine Laser (AGIL)," presented at 33rd AIAA Plasmadynamics and Lasers Conference, Maui, Hawaii, 2002.

[3] T. L. Henshaw, G. C. Manke II, T. J. Madden, M. R. Berman, and G. D. Hager, "A new energy transfer chemical laser at 1.315 μm," *Chem. Phys. Lett.*, vol. 325, pp. 537 - 544, 2000.

[4] J. M. Herbelin, T. L. Henshaw, B. D. Rafferty, B. T. Anderson, R. F. Tate, T. J. Madden, G. C. Manke, and G. D. Hager, "The measurement of gain on the 1.315 μm transition of atomic iodine in a subsonic flow of chemically generated NCl($a^1\Delta$)," *Chem. Phys. Lett.*, vol. 299, pp. 583-588, 1999.

[5] W. E. McDermott, N. R. Pchelkin, D. J. Benard, and R. R. Bousek, "An Electronic Transition Chemical Laser," *Appl. Phys. Lett*, vol. 32, pp. 469-470, 1978.

[6] W. E. McDermott, "Historical Perspective of COIL," presented at Proceedings of SPIE: Gas and Chemical Laser and Intense Beam Applications III, San Jose, CA, 2002.

[7] M. C. Heaven, "Chemical Dynamics in Chemical Laser Media," in *Chemical Dynamics in Extreme Environments*, *Advanced Series in Physical Chemistry*, R. A. Dressler, Ed.: World Scientific, 2001.

[8] "25 Years of COIL, Sessions 1 - 3," presented at Proceedings of SPIE: Gas And Chemical Lasers and Intense Beam Applications III, San Jose, CA, 2002.

[9] D. J. Benard, M. A. Chowdhury, B. K. Winker, T. A. Seder, and H. H. Michels, "Production of NCl(a) By Thermal-Decomposition of ClN_3," *Journal of Physical Chemistry*, vol. 94, pp. 7507-7514, 1990.

[10] R. D. Bower and T. T. Yang, "I($^2P_{1/2}$) Produced By the Energy-Transfer From Ncl($a^1\Delta$) to I($^2P_{3/2}$)," *J. Opt. Soc. Am. B*, vol. 8, pp. 1583-1587, 1991.

[11] T. T. Yang, V. T. Gylys, R. D. Bower, and L. F. Rubin, "Population inversion between I($^2P_{1/2}$) and I($^2P_{3/2}$) of atomic iodine generated by the energy transfer from NCl($a^1\Delta$) to I($^2P_{3/2}$)." *Opt. Lett.*, vol. 17, pp. 1803 - 1805, 1992.

[12] M. A. A. Clyne, A. J. MacRobert, J. Brunning, and C. T. Cheah, "Kinetics of metastable singlet NCl radicals," *J. Chem. Soc. Faraday Trans. 2*, vol. 79, pp. 1515 - 1524, 1983.

[13] M. A. A. Clyne and A. J. MacRobert, "Elementary reactions of the NCl radical. I. Rate constants for the reactions NCl+NCl to N_2+2Cl and O+NCl to NO+Cl.," *J. Chem. Soc. Faraday Trans. 2*, vol. 79, pp. 283 - 293, 1983.

[14] M. A. A. Clyne, A. J. Macrobert, and L. J. Stief, "Elementary Reactions of the NCl Radical .2. Kinetics of the NCl+ClO and NCl+NO Reactions," *Journal of the Chemical Society-Faraday Transactions Ii*, vol. 81, pp. 159-167, 1985.

[15] A. J. Ray and R. D. Coombe, "Energy-Transfer From NCl($a^1\Delta$) to Iodine Atoms," *J. Phys. Chem.*, vol. 97, pp. 3475-3479, 1993.

[16] A. J. Ray and R. D. Coombe, "An I* Laser-Pumped By NCl($a^1\Delta$)," *J. Phys. Chem.*, vol. 99, pp. 7849-7852, 1995.

[17] D. B. Exton, J. V. Gilbert, and R. D. Coombe, "Generation of Excited NCl By the Reaction of Hydrogen-Atoms With NCl_3," *Journal of Physical Chemistry*, vol. 95, pp. 2692-2696, 1991.

[18] J. V. Gilbert, X. L. Wu, D. H. Stedman, and R. D. Coombe, "Photolysis of Nitrogen Trichloride," *Journal of Physical Chemistry*, vol. 91, pp. 4265-4269, 1987.

[19] R. W. Schwenz, J. V. Gilbert, and R. D. Coombe, "NCl ($a^1\Delta$) and I ($5^2P_{1/2}$) Production in a D/NCl_3/Hi Transverse Flow Reactor," *Chemical Physics Letters*, vol. 207, pp. 526-530, 1993.

[20] A. V. Komissarov, G. C. Manke II, S. J. Davis, and M. C. Heaven, "Kinetic Spectroscopy of NCl," presented at Proceedings of SPIE: Gas Chemical, and Electrical Lasers and Intense Beam Applications., San Jose, CA, 2000.

[21] A. V. Komissarov, G. C. Manke II, S. J. Davis, and M. C. Heaven, "Rate Constants for Quenching and Self-Annihilation of NCl($a^1\Delta$)," *J. Phys. Chem. A*, vol. 106, pp. 8427 - 8434, 2002.

[22] T. L. Henshaw, S. D. Herrera, G. W. Haggquist, and L. A. V. Schlie, "Kinetics of Ncl($a^1\Delta$) Via Photodissociation of ClN_3," *J. Phys. Chem. A*, vol. 101, pp. 4048-4056, 1997.

[23] T. L. Henshaw, S. D. Herrera, and L. A. V. Schlie, "Temperature-Dependence of the NCl($a^1\Delta$)+I($^2P_{3/2}$) Reaction From 300 to 482 K," *J. Phys. Chem. A*, vol. 102, pp. 6239-6246, 1998.

[24] G. C. Manke II, T. L. Henshaw, T. J. Madden, and G. D. Hager, "Temperature dependence of the Cl + HN_3 reaction from 300 to 480 K," *Chem. Phys. Lett.*, vol. 310, pp. 111-120, 1999.

[25] G. C. Manke II, T. L. Henshaw, T. J. Madden, and G. D. Hager, "Temperature-Dependent Quenching Rate Constants of NF($a^1\Delta$)," *J. Phys. Chem. A*, vol. 104, pp. 1708 - 1714, 2000.

[26] K. Y. Du and D. W. Setser, "Quenching Rate Constants of NF($a^1\Delta$) At Room-Temperature," *J. Phys. Chem.*, vol. 94, pp. 2425-2435, 1990.

[27] G. C. Manke II and D. W. Setser, "Kinetics of NCl($a^1\Delta$ and $b^1\Sigma^+$) Generation: The Cl + N_3 Rate Constant, the NCl($a^1\Delta$) Product Branching Fraction , and Quenching of NCl($a^1\Delta$) by F and Cl Atoms," *J. Phys. Chem. A*, vol. 102, pp. 7257-7266, 1998.

[28] G. C. Manke II and D. W. Setser, "Measuring Gas-Phase Chlorine Atom Concentrations : Rate Constants For Cl+HN_3 ; CF_3I ; and C_2F_5I," *J. Phys. Chem. A*, vol. 102, pp. 153-159, 1998.

[29] Y. Zhao and D. W. Setser, "Quenching Rate Constants For NCl($b^1\Sigma^+$) and PCl($b^1\Sigma^+$) and Radiative Lifetimes of NCl($b^1\Sigma^+$) and PBr($b^1\Sigma^+$)," *Journal of the Chemical Society-Faraday Transactions*, vol. 91, pp. 2979-2987, 1995.

[30] K. B. Hewett, G. C. Manke II, D. W. Setser, and G. Brewood, "Quenching Rate Constants of NCl($a^1\Delta$) at Room Temperature," *J. Phys. Chem. A.*, vol. 104, pp. 539 - 551, 2000.

[31] K. B. Hewett and D. W. Setser, "Chemical-Kinetics of the Azide Radical : Rate Constants For Reactions With Cl ; NO ; NO2 ; O_2 ; CO ; CO_2 ; Cl_2 ; and C_3H_6," *J. Phys. Chem. A*, vol. 102, pp. 6274-6281, 1998.

[32] G. C. Manke II, "unpublished results," 2004.

[33] L. Duo, S. Tang, J. Li, X. Min, F. Sang, and B. Yang, "Parametric Study of NCl($a^1\Delta$), NCl($b^1\Sigma$) from the reaction of $Cl/Cl_2/He + HN_3/He$," presented at Proceedings of SPIE: Gas and Chemical Lasers and Intense Beam Applications III, San Jose, CA, 2002.

[34] G. C. Manke II, T. L. Henshaw, T. J. Madden, J. M. Herbelin, B. D. Rafferty, and G. D. Hager, "Characterizing fluorine and chlorine atom flow rates using iodine atom spectrometry," *AIAA Journal*, vol. 39, pp. 447 - 454, 2001.

[35] S. J. Davis, P. A. Mulhall, W. J. Kessler, M. C. Heaven, and G. C. Manke II, "Diode laser-based diagnostic for NCl(X)," presented at Proceedings of SPIE: Gas and Chemical Lasers and Intense Beam Applications IV, San Jose, CA, 2003.

[36] A. C. Becker and U. Schurath, "Matrix-Isolated NCl : Radiative Rates For $b^1\Sigma^+$- $a^1\Delta$;$b^1\Sigma^+$- $X^3\Sigma^-$ and $a^1\Delta$ - $X^3\Sigma^-$ in Solid Argon," *Chem. Phys. Lett.*, vol. 160, pp. 586-590, 1989.

[37] S. J. Davis, W. J. Kessler, and M. Bachmann, "Collisional broadening of absorption lines in water vapor and atomic iodine relevant to COIL diagnostics," *Proc. SPIE - Int. Soc. Opt. Eng.*, vol. 3612, pp. 157 - 166, 1999.

[38] S. J. Davis, W. J. Kessler, and P. B. Keating, "Progress in the development of sensors for COIL devices," *Proc. SPIE - Int. Soc. Opt. Eng.*, vol. 3931, pp. 156 - 161, 2000.

[39] S. Gerstenkorn and P. Luc, *Atlas Du Spectre D'Absorption de la Molecule D'Iode*. Paris: Editions du CNRS, 1978.

[40] Lasing on the AGIL 1 and 2 devices was achieved with g = 1 – 4 x 10-4 cm-1 and the recent ElectriCOIL lasing demonstration by Carroll and co-workers was accomplished with g = 6 x 10-5 cm-1

Distribution List

DTIC/OCP 8725 John J. Kingman Rd, Suite 0944 Ft Belvoir, VA 22060-6218	1 cy
AFRL/VSIL Kirtland AFB, NM 87117-5776	2 cys
AFRL/VSIH Kirtland AFB, NM 87117-5776	1 cy
Official Record Copy AFRL/DELC/Gerald Manke	1 cy
AFOSR Michael Berman	1 cy
MDA/AL Keith Truesdell	1 cy
MDA/AS James Mulroy	1 cy
DARPA Sheldon Meth	1 cy
JTO Mark Neice	1 cy
SAF/AQR Col Mark Stephen	1 cy